



Cochlea-Specific Deletion of Ca_v1.3 Calcium Channels Arrests Inner Hair Cell Differentiation and Unravels Pitfalls of Conditional Mouse Models

Stephanie Eckrich¹, Dietmar Hecker², Katharina Sorg², Kerstin Blum¹, Kerstin Fischer¹, Stefan Münkner¹, Gentiana Wenzel², Bernhard Schick² and Jutta Engel^{1*}

¹ Department of Biophysics, Center for Integrative Physiology and Molecular Medicine (CIPMM), School of Medicine, Saarland University, Homburg, Germany, ² Department of Otorhinolaryngology, Saarland University, Homburg, Germany

OPEN ACCESS

Edited by:

Josef Bischofberger,
Universität Basel, Switzerland

Reviewed by:

Petronel Tuluc,
University of Innsbruck, Austria
Joshua Singer,
University of Maryland, College Park,
United States

*Correspondence:

Jutta Engel
jutta.engel@uni-saarland.de

Specialty section:

This article was submitted to
Cellular Neurophysiology,
a section of the journal
Frontiers in Cellular Neuroscience

Received: 07 March 2019

Accepted: 03 May 2019

Published: 22 May 2019

Citation:

Eckrich S, Hecker D, Sorg K,
Blum K, Fischer K, Münkner S,
Wenzel G, Schick B and Engel J
(2019) Cochlea-Specific Deletion
of Ca_v1.3 Calcium Channels Arrests
Inner Hair Cell Differentiation
and Unravels Pitfalls of Conditional
Mouse Models.
Front. Cell. Neurosci. 13:225.
doi: 10.3389/fncel.2019.00225

Inner hair cell (IHC) Ca_v1.3 Ca²⁺ channels are multifunctional channels mediating Ca²⁺ influx for exocytosis at ribbon synapses, the generation of Ca²⁺ action potentials in pre-hearing IHCs and gene expression. IHCs of deaf systemic Ca_v1.3-deficient (Ca_v1.3^{-/-}) mice stay immature because they fail to up-regulate voltage- and Ca²⁺-activated K⁺ (BK) channels but persistently express small conductance Ca²⁺-activated K⁺ (SK2) channels. In pre-hearing wildtype mice, cholinergic neurons from the superior olivary complex (SOC) exert efferent inhibition onto spontaneously active immature IHCs by activating their SK2 channels. Because Ca_v1.3 plays an important role for survival, health and function of SOC neurons, SK2 channel persistence and lack of BK channels in systemic Ca_v1.3^{-/-} IHCs may result from malfunctioning neurons of the SOC. Here we analyze cochlea-specific Ca_v1.3 knockout mice with green fluorescent protein (GFP) switch reporter function, *Pax2::cre;Cacna1d-eGFP^{flex/lex}* and *Pax2::cre;Cacna1d-eGFP^{flex/-}*. Profound hearing loss, lack of BK channels and persistence of SK2 channels in *Pax2::cre;Cacna1d-eGFP^{flex/-}* mice recapitulated the phenotype of systemic Ca_v1.3^{-/-} mice, indicating that in wildtype mice, regulation of SK2 and BK channel expression is independent of Ca_v1.3 expression in SOC neurons. In addition, we noticed dose-dependent GFP toxicity leading to death of basal coil IHCs of *Pax2::cre;Cacna1d-eGFP^{flex/lex}* mice, likely because of high GFP concentration and small repair capacity. This and the slower time course of *Pax2*-driven Cre recombinase in switching two rather than one *Cacna1d-eGFP^{flex}* allele lead us to study *Pax2::cre;Cacna1d-eGFP^{flex/-}* mice. Notably, control *Cacna1d-eGFP^{flex/-}* IHCs showed a significant reduction in Ca_v1.3 channel cluster sizes and currents, suggesting that the intronic construct interfered with gene translation or splicing. These pitfalls are likely to be a frequent problem of many genetically modified mice with complex or multiple gene-targeting constructs or fluorescent proteins. Great caution and appropriate controls are therefore required.

Keywords: inner hair cell, Ca²⁺ channel, Ca_v1.3, BK, conditional knockout, flex switch, GFP toxicity, hearing

INTRODUCTION

The L-type calcium (Ca²⁺) channel Ca_v1.3 is the main voltage-gated Ca²⁺ channel (VGCC) in inner hair cells (IHCs) and essential for hearing (Platzer et al., 2000; Baig et al., 2011). In both pre-hearing and mature IHCs, voltage-activated Ca_v1.3 channels trigger glutamate release resulting in signal transmission to the auditory nerve (Brandt et al., 2003). Before the onset of hearing at postnatal day 12 in mice, IHCs produce spontaneous Ca²⁺-action potentials (Kros et al., 1998; Platzer et al., 2000; Marcotti et al., 2003) required for the terminal differentiation of IHCs (Brandt et al., 2003; Nemzou et al., 2006; Johnson et al., 2013a) and maturation of the auditory brainstem (Tritsch and Bergles, 2010; Clause et al., 2014; Babola et al., 2018). IHC spontaneous activity is modulated by transient efferent input originating in the superior olivary complex (SOC), which activates small-conductance SK2 potassium (K⁺) channels and thereby causes hyperpolarization of the IHC membrane potential (Glowatzki and Fuchs, 2000; Oliver et al., 2000). Around the onset of hearing, IHCs lose their efferent input (Simmons, 2002), SK2 channels are down-regulated (Marcotti et al., 2004) and spontaneous activity ends with the up-regulation of BK and KCNQ4 K⁺ channels (Kros et al., 1998; Oliver et al., 2003). IHCs of systemic Ca_v1.3^{-/-} mice fail to acquire a mature composition of K⁺ channels (Brandt et al., 2003; Nemzou et al., 2006), which is likely caused by lack of spontaneous activity and impaired Ca²⁺-dependent transcriptional regulation. However, altered efferent modulation due to lack of Ca_v1.3 in brainstem nuclei might add to the phenotype. Ca_v1.3 plays an intrinsic role for development and function of SOC neurons (Hirtz et al., 2011, 2012; Satheesh et al., 2012) and is therefore regarded not only as a peripheral but also a central deafness gene (Willaredt et al., 2014).

Here, the effects of cochlea-specific ablation of Ca_v1.3 channels before birth on the electrophysiological and molecular phenotype of IHCs as well as hearing function were investigated. To this end, *Cacna1d-eGFP^{flex}* mice were used, in which the ablation of *Cacna1d* encoding Ca_v1.3 channels is directly coupled to the expression of the reporter gene *eGFP* via Cre-induced inversion (“switch”) of the floxed allele (Satheesh et al., 2012). They were crossed with *Pax2::cre* mice (Ohyama and Groves, 2004), where Cre expression is initiated at E9.5 in the otic vesicle (Lawoko-Kerali et al., 2001; Burton et al., 2004) and found in the mature organ of Corti and spiral ganglion neurons (SGN) but not in the nuclei that are part of the afferent-efferent feedback loop onto hair cells, i.e., ventral cochlear nucleus and the SOC (Zuccotti et al., 2012).

MATERIALS AND METHODS

Animals

Cacna1d-eGFP^{flex} mice were generated within the *CavNET* consortium (EU-CAVNET MRTN-CT-2006-035367) by Katrin Bartels née Kunert, Kai Schönig and Dusan Bartsch, Central Institute of Mental Health, Mannheim, Germany (Satheesh et al., 2012). They were cross-bred with *Cacna1d^{-/-}* mice (Platzer et al., 2000) and *Pax2::cre* mice (Ohyama and Groves, 2004;

Zuccotti et al., 2012). To reduce the risk of unwanted effects caused by Cre expression, only mice heterozygous for *Pax2::cre* were used (Jae Huh et al., 2010; Janbandhu et al., 2014). Animals were housed with free access to food and water at an average temperature of 22°C and a 12 h light-dark cycle. Mice of either sex were sacrificed by decapitation under isoflurane anesthesia and their cochleae were dissected from the temporal bones. All experiments were carried out in accordance with the European Communities Council Directive (86/609/EEC) and approved by the regional board for scientific animal experiments of the Saarland, Germany. Additional ethics approval was not required according to the local and national guidelines.

Genotyping

The *Pax2::cre* allele was genotyped using primers detecting *Cre*: 5'-GCC TGC ATT ACC GGT CGA TGC AAC GA-3' and 5'-GTG GCA GAT GGC GCG GCA ACA CCA TT-3' (product size: 726 bp). The *Cacna1d-eGFP^{flex}* (“*flex*”) allele was identified using: 5'-TTC AAG GAC GAC GGC AAC TAC AAG-3' and 5'-CGG CGG CGG TCA CGA ACT CC-3' (product size: 380 bp). To exclude accidental occurrence of unwanted embryonal or germline recombination of the *flex* allele in pups without Cre, we regularly used the following primers: “*Flex A*” (5'-GGA GTT GTG TAT ATC TGT TAA GCC ATG-3'), “*Flex B*” (5'-GCT GTT GGG CTG AGA AGT TGG T-3') and “*Flex C*” (5'-CCA GAA GAT TCC ACT AAA GGT CAT-3'), detecting wildtype (*A-B* band, ~450 bp), intact *flex* (*A-B* band, ~600 bp) and switched *flex* allele (*B-C* band, ~700 bp) (Bartels, 2009). The *Cacna1d⁻* (“Ca_v1.3⁻”) allele was genotyped with the primers: “*Ca_v1.3 sense (s)*” (5'-GCA AAC TAT GCA AGA GGC ACC AGA-3'), “*Ca_v1.3 antisense (as)*” (5'-TAC TTC CAT TCC ACT ATA CTA ATG CAG GCT-3') and “*Ca_v1.3 neosense (ns)*” (5'-TTC CAT TTG TCA CGT CCT GCA CCA-3') yielding a wildtype (*s-as*, ~300 bp) and/or a knockout band (*s-ns*, ~450 bp).

Hearing Measurements

Auditory brainstem responses (ABR) and distortion product otoacoustic emissions (DPOAE) were recorded in anesthetized mice aged 4–6 weeks as described in Fell et al. (2016). Growth functions of ABR waves I to IV in response to click stimuli were analyzed for peak-to-peak amplitudes and latencies between the click stimulus delivered at *t* = 0 and the time point of the negative peak of the respective wave.

Electrophysiological Recordings

Apical-turn organs of Corti were acutely dissected from young adult mice (P17–P23) in solution containing (in mM): 70 lactobionate-NaOH, 83 NaCl, 10 HEPES, 5.8 KCl, 5.3 glucose, 1.3 CaCl₂, 0.95 MgCl₂, 0.7 NaH₂PO₄. For Ba²⁺ current recordings, the bath solution contained (in mM): 72.5 lactobionate-NaOH, 40 NaCl, 35 TEA, 15 4-AP, 10 BaCl₂, 10 HEPES, 5.6 glucose, 0.9 MgCl₂. Both solutions were adjusted to pH 7.35, 320 mosmol kg⁻¹. Quartz pipettes were used and filled with (in mM): 112 Cs⁺ methane sulfonate, 20 CsCl, 10 Na⁺ phosphocreatine, 5 HEPES, 1 EGTA, 4 MgCl₂, 4 Na₂ATP, 0.3 GTP, 0.1 CaCl₂. Pipette solution was adjusted to pH 7.36, 305 mosmol kg⁻¹.

Before performing whole-cell patch clamp recordings using an Optopatch (Cairn Research, United Kingdom) or an Axopatch 200B amplifier (Molecular Devices, United States), green fluorescent protein (GFP) fluorescence of the specimen was assessed with an epifluorescence system consisting of a UV lamp and FITC fluorescence filters attached to the patch microscope (Olympus BX51WI with a 40 x water immersion objective, Germany) and a CCD camera (Scientifica, United Kingdom). Ba²⁺ currents were elicited by depolarizing the cells for 8 ms from -98 to +48 mV in 5 mV increments. Uncompensated series resistance was corrected by 70–80%. Analysis, including off-line linear leak subtraction and correction of the currents by subtracting the liquid junction potential of 8 mV, was performed using Igor Pro software (Wavemetrics, United States). *I-V* relations were calculated as the average current taken from the last ms of the voltage step as a function of the respective voltage.

I-V curves of Ba²⁺ currents were fitted to a second-order Boltzmann function times Goldman-Hodgkin-Katz driving force to determine parameters of activation, the voltage of half-maximum activation, *V*_h, and the voltage sensitivity of activation determined by the slope factor *k*, according to

$$I = -P_{\max} z F v \left(\frac{[Ba]_o}{e^{v-1}} + \frac{[Ba]_i}{e^{-(v+1)}} \right) \cdot \left(\frac{1}{1 + e^{\frac{(v_h - v)}{k}}} \right)^2 \quad (1)$$

where *I* is *I*_{Ba} at the time point the *I-V* was calculated (average over 7–8 ms after depolarization); *P*_{max} the maximum permeability; *v* = *zFV*/(*RT*), with *z* being 2, *F* the Faraday constant, *R* the universal gas constant, *T* the absolute temperature, *V* the membrane potential. *[Ba]*_i (set at 50 nM) and *[Ba]*_o denote the intra- and extracellular Ba²⁺ concentration, respectively.

Immunohistochemistry

Immunolabeling was performed on whole-mount organs of Corti of 4–6 week-old mice as described in Fell et al. (2016) using Zamboni's fixative for 8 min on ice. Specimens were labeled using antibodies against Ca_v1.3 (rabbit polyclonal, Alomone Labs, Israel, 1:500), BKα (rabbit polyclonal, Alomone Labs, Israel, 1:500; mouse monoclonal, antibodies-online, Germany, 1:500), GFP (goat polyclonal, Rockland, United States, 1:500), CtBP2/RIBEYE (mouse monoclonal, BD Transduction Laboratories, Germany, 1:100 – 1:200), SK2 (rabbit polyclonal, Sigma-Aldrich, Germany, 1:400), and calbindin (rabbit polyclonal, Swant Inc., Switzerland, 1:400). Primary antibodies were detected with Cy3-conjugated (donkey anti-rabbit: Jackson Immuno Research Laboratories, United Kingdom, 1:1500; donkey anti-goat: Abcam, United Kingdom, 1:1500) or Alexa 488-conjugated (anti-mouse: Invitrogen, United Kingdom, 1:500; anti-goat: Abcam, United Kingdom, 1:500) secondary antibodies. For immunolabeling experiments, at least three specimens of ≥3 animals were analyzed. *z*-stacks of fluorescence images were acquired using a confocal laser scanning microscope LSM710 (Carl Zeiss Microscopy GmbH, Germany). Images were analyzed with Fiji (Schindelin et al., 2012).

For quantification of Ca_v1.3 clusters and RIBEYE-positive ribbons, images of 67.5 μm × 38.9 μm size covering eight IHCs were acquired at equal laser and gain settings, and maximum intensity projections (MIPs) were calculated. The channel of interest of a MIP image was background subtracted. A thresholded binary image was created (0 below threshold; 1 above threshold) with thresholds of 10% of the maximum intensity of the green color channel (RIBEYE) and 17% of the red color channel (Ca_v1.3). Fluorescent dots < 0.05 μm² were discarded. Size and number of clusters were analyzed using the particle count routine in Fiji and normalized to one IHC.

Statistics

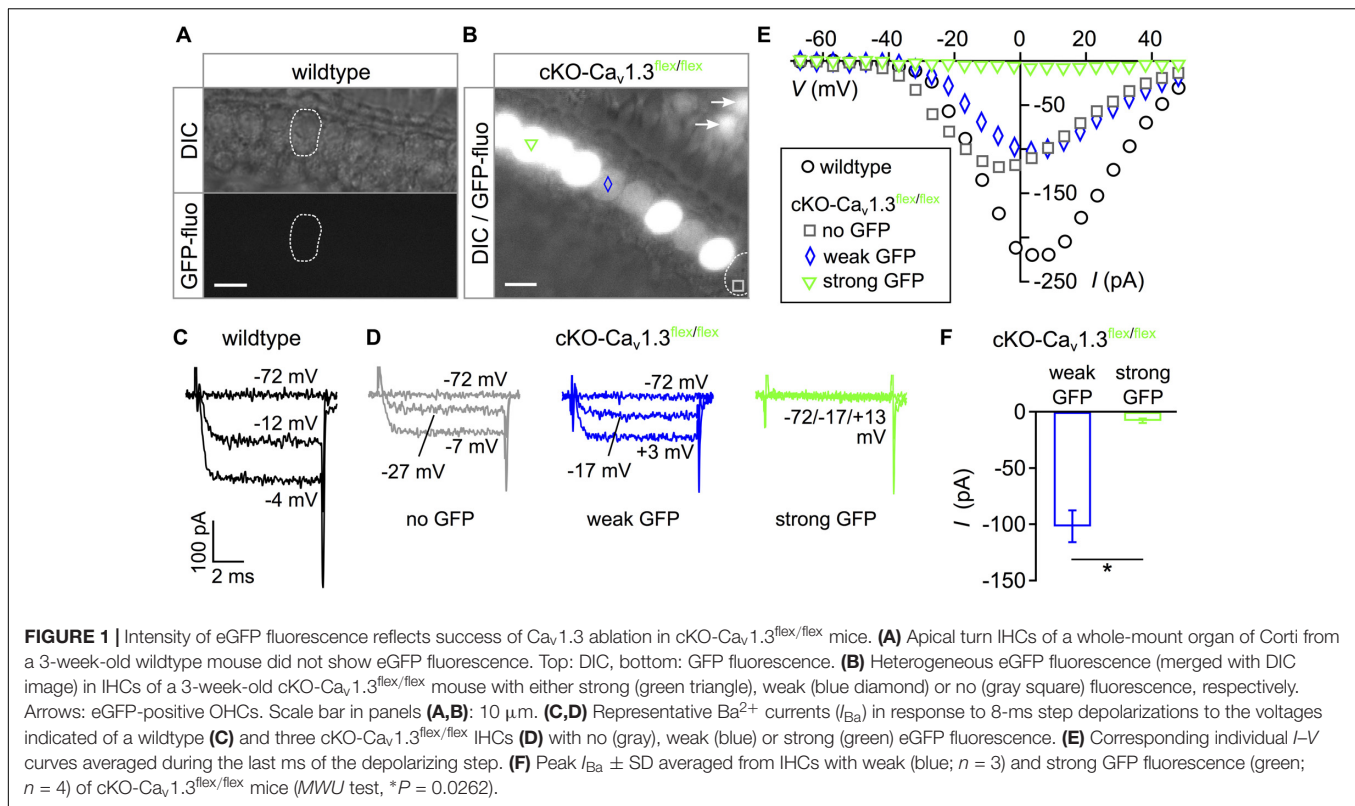
Data are provided as mean ± SD, unless otherwise stated. Depending on the distribution of the data, Ba²⁺ current properties, as well as size and number of Ca_v1.3 clusters and ribbons were statistically analyzed using Student's *t*-test or Mann-Whitney *U* test (*MWU* test; comparison of two groups) or using one-way ANOVA followed by Tukey *post hoc* test or Kruskal-Wallis test followed by Dunn-Holland-Wolfe *post hoc* test (comparison of > 2 groups) with Igor Pro software (WaveMetrics, United States) and SPSS statistics (IBM, Germany).

Statistical analysis of hearing measurements was performed with SPSS. Click ABR thresholds were analyzed using a one-way ANOVA, DPOAE amplitudes with a Kruskal-Wallis test and frequency-dependent ABR thresholds with a two-way ANOVA; all tests were followed by a Bonferroni *post hoc* test. ABR growth functions of amplitudes and latencies could not be tested by a two-way ANOVA due to unequal variances. Instead, a regression analysis was performed, and the parameters of the resulting regression lines (slope and *y*-axis intercept) were tested for differences using Student's *t*-test or *MWU* test according to Sachs (1999).

RESULTS

Cochlea-Specific Deletion of the Ca_v1.3 Channel Using Ca_v1.3-*flex* Mice With Cre Expression Under the *Pax2* Promoter

In order to assess the phenotype of mice with cochlea-specific ablation of *Cacna1d* before birth, we analyzed GFP signals and whole-cell Ba²⁺ currents through Ca_v1.3 channels in IHCs of conditional knockout (cKO) *Pax2::cre;Cacna1d-eGFP^{flex/lex}* mice, in short cKO-Ca_v1.3^{flex/lex}. GFP fluorescence of two distinct intensity levels was present in IHCs of the apical cochlear turn acutely dissected from 3-week-old cKO-Ca_v1.3^{flex/lex} mice (Figure 1B) but not in wildtype IHCs (Figure 1A). Analysis of Ba²⁺ currents (*I*_{Ba}) using 10 mM Ba²⁺ as a charge carrier in response to 8 ms step depolarizations revealed lack of *I*_{Ba} exclusively in those IHCs with a strong GFP signal (Figure 1D, green trace). In contrast, *I*_{Ba} was present in one IHC of cKO-Ca_v1.3^{flex/lex} mice with weak (blue trace), one IHC without GFP fluorescence (gray trace, Figure 1D) and a wildtype IHC (Figure 1C). Corresponding individual peak *I-V* relations show



that *I*_{Ba} was abolished in the IHC with strong GFP fluorescence whereas it was present in the two cKO-Ca_v1.3^{flex/flex} IHCs with weak or no GFP fluorescence and in the wildtype IHC (**Figure 1E**). Averaged peak *I*_{Ba} from cKO-Ca_v1.3^{flex/flex} IHCs with strong GFP (-7.9 ± 1.9 pA; *n* = 4) was significantly reduced compared with IHCs showing weak GFP fluorescence (-101.6 ± 14.2 pA; *n* = 3; *P* = 0.0262, *MWU* test, **Figure 1F**). We concluded that only those IHCs with strong fluorescence represented true knockout cells with two switched *flex* alleles whereas IHCs with weak fluorescence represented cells with one switched and one intact *flex* allele.

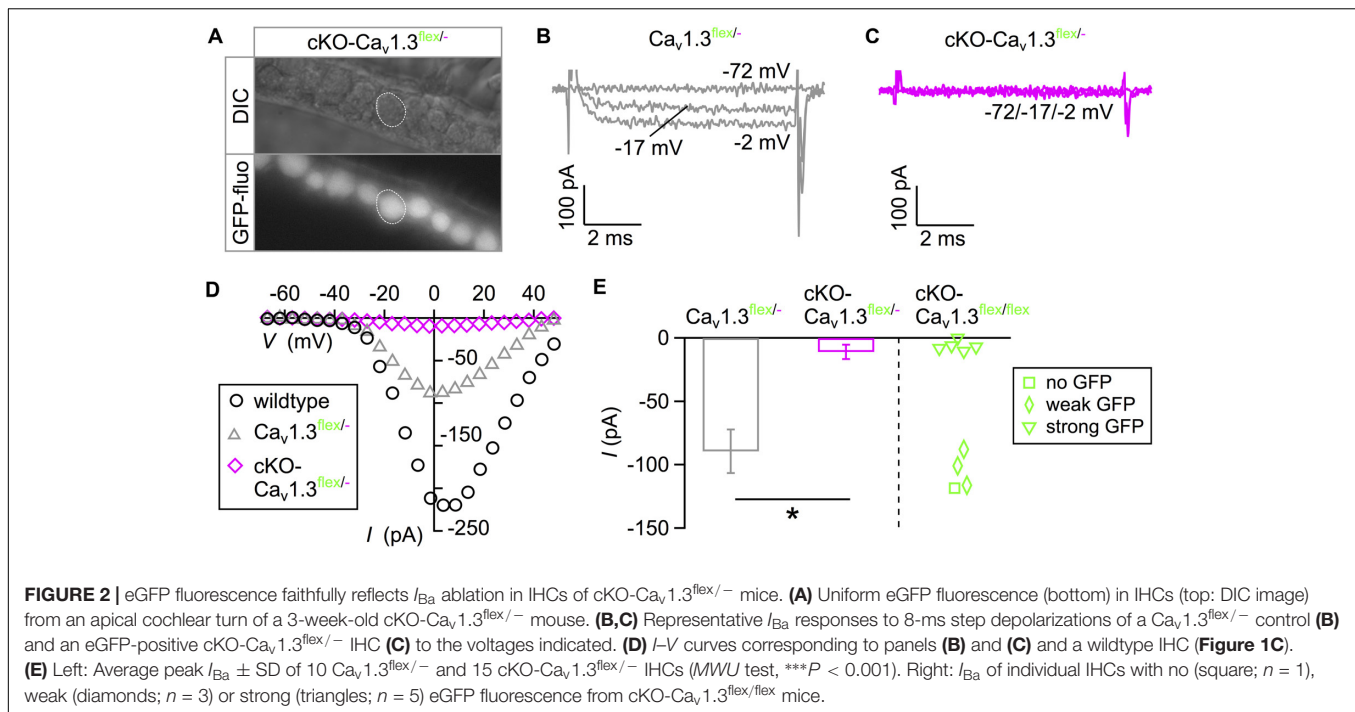
In order to increase the ratio of “true knockout” IHCs without remaining intact *flex* alleles, cKO-Ca_v1.3^{flex/flex} mice were crossbred with Ca_v1.3^{-/-} mice resulting in cKO-Ca_v1.3^{flex/-} mice, in which Cre needed to cut and switch only one *flex* allele per cell. Here, GFP fluorescence was uniform in IHCs of acutely dissected organs of Corti from 3-week-old cKO-Ca_v1.3^{flex/-} mice (**Figure 2A**). Typical *I*_{Ba} traces (**Figures 2B,C**) and corresponding *I*-*V* curves (**Figure 2D**) show that *I*_{Ba} was abolished in GFP-positive IHCs of cKO-Ca_v1.3^{flex/-} mice (**Figure 2C**) but retained in control IHCs of Ca_v1.3^{flex/-} mice (**Figure 2B**) where the *flex* allele was not switched due to absence of Cre. *I*-*V* curves further showed a reduction of *I*_{Ba} in control Ca_v1.3^{flex/-} (gray) compared with wildtype IHCs (black, **Figure 2D**). The average peak *I*_{Ba} from cKO-Ca_v1.3^{flex/-} IHCs was significantly reduced compared with control Ca_v1.3^{flex/-} IHCs (**Figure 2E**, bars; *MWU* test, *P* < 0.001). Peak *I*_{Ba} from individual cKO-Ca_v1.3^{flex/flex} IHCs demonstrate that the *I*_{Ba} amplitude of IHCs with strong GFP fluorescence (cf. **Figure 1**

resembled that of GFP-positive IHCs of cKO-Ca_v1.3^{flex/-} mice whereas *I*_{Ba} values of IHCs with weak or no GFP fluorescence were similar to those of Ca_v1.3^{flex/-} IHCs (**Figure 2E**, right). The lack of *I*_{Ba} was accompanied by a reduction in cell size as evident by a significantly reduced membrane capacitance (*P* < 0.001, Kruskal-Wallis Test) in cKO-Ca_v1.3^{flex/-} mice (6.7 ± 0.6 pF; *n* = 15; *P* = 0.001, effect of genotype) but not in control Ca_v1.3^{flex/-} mice (9.5 ± 1.4 pF; *n* = 10) compared with the wildtype (8.7 ± 1.0 pF; *n* = 10).

In summary, heterogeneous GFP expression and persistence of *I*_{Ba} in IHCs with weak GFP fluorescence of cKO-Ca_v1.3^{flex/flex} mice show that (i) Cre did not faithfully switch both *flex* alleles at 3 weeks of age and (ii) GFP fluorescence is no reliable marker for deletion of Ca_v1.3 channels in IHCs of cKO-Ca_v1.3^{flex/flex} mice. In contrast, in IHCs of cKO-Ca_v1.3^{flex/-} mice containing only one *flex* allele, GFP fluorescence unequivocally indicated a cellular knockout genotype.

GFP Toxicity in IHCs of cKO-Ca_v1.3^{flex/flex} Mice

In Ca_v1.3^{-/-} mice, mild degeneration of IHCs has been reported in the apical cochlear turn starting after P20 and in the basal cochlear turn after P35 (Platzer et al., 2000; Glueckert et al., 2003; Nemzou et al., 2006). Degeneration of IHCs after cochlea-specific deletion of Ca_v1.3 was analyzed in organs of Corti of 4–5 week-old cKO-Ca_v1.3^{flex/flex} and cKO-Ca_v1.3^{flex/-} compared with Ca_v1.3^{-/-} mice, which were double-immunolabeled for GFP and the hair-cell marker calbindin (**Figure 3** and **Table 1**).



IHCs of all three genotypes showed mild IHC loss of $\leq 6.3\%$ in the apical turn (**Figures 3A–C** and **Table 1**). In contrast, the majority (81.3%) of basal-turn IHCs of cKO- $Ca_v1.3^{flex/flex}$ mice was missing (**Figure 3E** and **Table 1**). This pronounced degeneration was not caused by lack of $Ca_v1.3$ because basal-turn IHCs of $Ca_v1.3^{-/-}$ and cKO- $Ca_v1.3^{flex/-}$ mice did not show any degeneration ($< 0.5\%$; **Figures 3D,F** and **Table 1**). We conclude that high expression levels of GFP caused by two functional *flex* alleles in cKO- $Ca_v1.3^{flex/flex}$ mice (cf. **Figure 1A**) resulted in a toxic effect of GFP on basal IHCs. The lack of IHC degeneration in the basal cochlea from cKO- $Ca_v1.3^{flex/-}$ mice suggests a dose-dependent toxicity of GFP that requires more than one functional GFP allele.

The majority of outer hair cells (OHCs) from the apical (**Figures 3A–C**) but not basal cochlear turn (**Figures 3D–F**) were degenerated, as described before for $Ca_v1.3^{-/-}$ mice (Platzer et al., 2000; Glueckert et al., 2003; Engel et al., 2006). Thus, cochlea-specific deletion of $Ca_v1.3$ channels coupled to GFP expression resulted in a similar degeneration of apical turn OHCs as observed in systemic $Ca_v1.3^{-/-}$ mice.

The patterns of IHC GFP labeling in either cKO- $Ca_v1.3^{flex/flex}$ (**Figures 3B,E**) or cKO- $Ca_v1.3^{flex/-}$ mice (**Figures 3C,F**) were similar to the eGFP fluorescence patterns in acutely dissected organs of Corti from these genotypes (**Figures 1A, 2A**). GFP labeling intensity was heterogeneous between individual IHCs of cKO- $Ca_v1.3^{flex/flex}$ mice with either intense or weak (arrows) labeling (**Figures 3B,E**) but uniform in IHCs of cKO- $Ca_v1.3^{flex/-}$ mice (**Figures 3C,F**), with few individual IHCs not being labeled (**Figure 3C**, arrowheads).

The rate of true knockout IHCs was assessed by quantification of apical-turn organs of Corti immunolabeled for GFP, $Ca_v1.3$ and/or BK channels (**Table 2**). In cKO- $Ca_v1.3^{flex/-}$ mice, the

knockout rate was 89.2%, which was only slightly higher than the knockout rate of 87.4% in cKO- $Ca_v1.3^{flex/flex}$ mice at 4–5 weeks of age. Although replacing one *flex* allele by a knockout (–) allele increased the success rate of Cre in switching one *flex* allele at 3 weeks of age (cf. **Figures 1A,B, 2A**), Cre caught up in switching both *flex* alleles in cKO- $Ca_v1.3^{flex/flex}$ mice 2 weeks later.

In conclusion, the percentage of knockout IHCs finally was not increased by replacement of one *flex* allele with a knockout (–) allele to obtain cKO- $Ca_v1.3^{flex/-}$ mice. However, we found that in cKO- $Ca_v1.3^{flex/flex}$ mice (i) basal-turn IHCs degenerated, most likely due to dose-dependent GFP toxicity and (ii) GFP expression in IHCs was not unequivocally associated with deletion of $Ca_v1.3$ channels, thus leading us to further use cKO- $Ca_v1.3^{flex/-}$ instead of cKO- $Ca_v1.3^{flex/flex}$ mice.

Similar Phenotypes of IHCs From cKO- $Ca_v1.3^{flex/-}$ and Systemic $Ca_v1.3^{-/-}$ Mice

In wildtype mice, up-regulation of BK K⁺ channels around the onset of hearing (P12) and down-regulation of neonatal SK2 K⁺ channels mark the end of terminal maturation and the onset of the mature function of IHCs (**Figure 4A**) (Kros et al., 1998; Marcotti et al., 2004). In systemic $Ca_v1.3^{-/-}$ mice, IHCs maintain an immature-like ion channel composition with persistent expression of SK2 but lack of BK K⁺ channels (Brandt et al., 2003; Engel et al., 2006; Nemzou et al., 2006). The failure of acquiring a mature composition of K⁺ channels may have been caused by lack of $Ca_v1.3$ currents (i) in the IHC itself or (ii) in brainstem nuclei causing an altered efferent input on the IHC (Hirtz et al., 2011, 2012; Sathesh et al., 2012). Precise

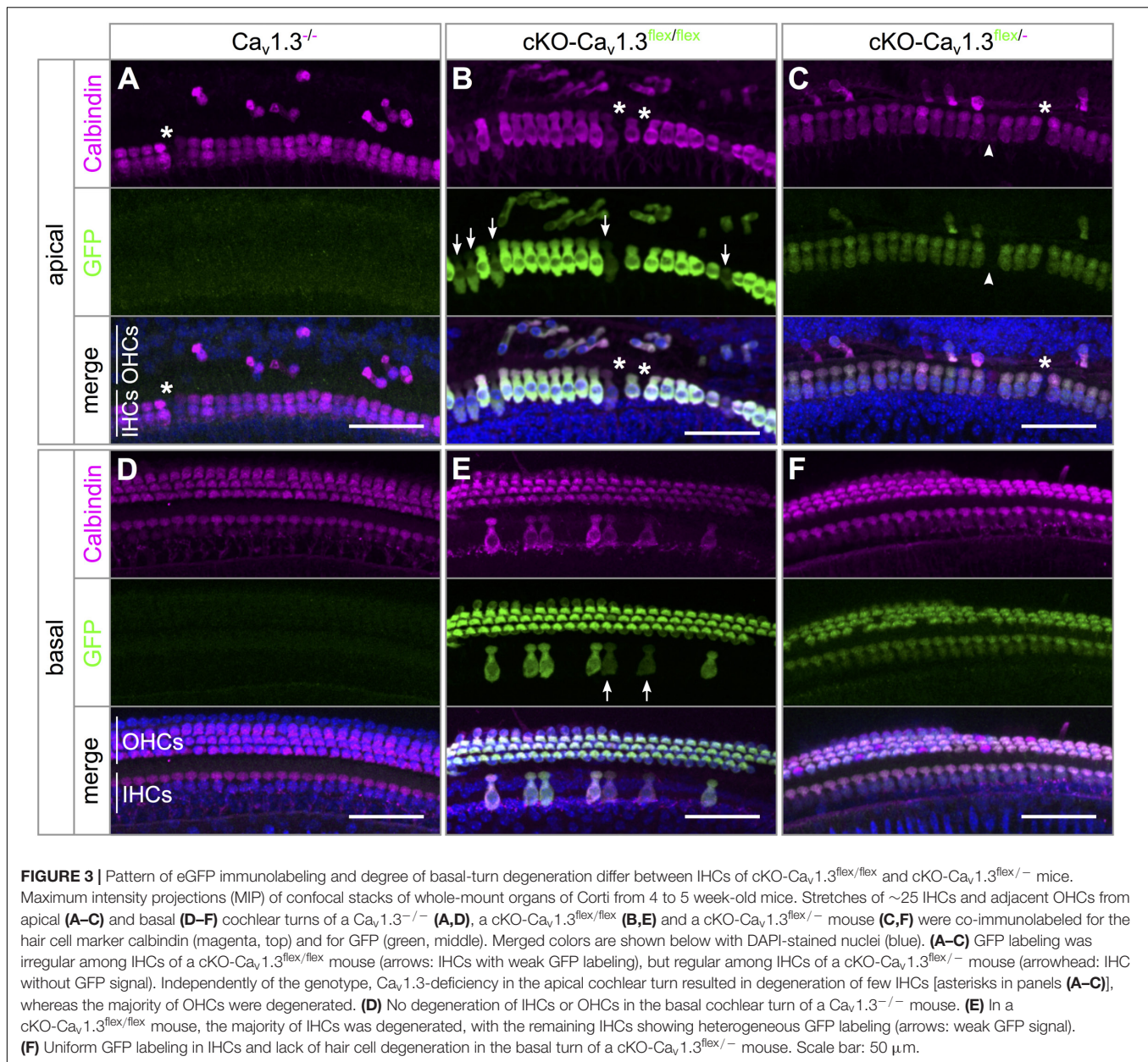


FIGURE 3 | Pattern of eGFP immunolabeling and degree of basal-turn degeneration differ between IHCs of cKO- $Ca_v1.3^{flex/flux}$ and cKO- $Ca_v1.3^{flex/-}$ mice. Maximum intensity projections (MIP) of confocal stacks of whole-mount organs of Corti from 4 to 5 week-old mice. Stretches of ~25 IHCs and adjacent OHCs from apical (**A–C**) and basal (**D–F**) cochlear turns of a $Ca_v1.3^{-/-}$ (**A,D**), a cKO- $Ca_v1.3^{flex/flux}$ (**B,E**) and a cKO- $Ca_v1.3^{flex/-}$ mouse (**C,F**) were co-immunolabeled for the hair cell marker calbindin (magenta, top) and for GFP (green, middle). Merged colors are shown below with DAPI-stained nuclei (blue). (**A–C**) GFP labeling was irregular among IHCs of a cKO- $Ca_v1.3^{flex/flux}$ mouse (arrows: IHCs with weak GFP labeling), but regular among IHCs of a cKO- $Ca_v1.3^{flex/-}$ mouse (arrowhead: IHC without GFP signal). Independently of the genotype, $Ca_v1.3$ -deficiency in the apical cochlear turn resulted in degeneration of few IHCs [asterisks in panels (**A–C**)], whereas the majority of OHCs were degenerated. (**D**) No degeneration of IHCs or OHCs in the basal cochlear turn of a $Ca_v1.3^{-/-}$ mouse. (**E**) In a cKO- $Ca_v1.3^{flex/flux}$ mouse, the majority of IHCs was degenerated, with the remaining IHCs showing heterogeneous GFP labeling (arrows: weak GFP signal). (**F**) Uniform GFP labeling in IHCs and lack of hair cell degeneration in the basal turn of a cKO- $Ca_v1.3^{flex/-}$ mouse. Scale bar: 50 μ m.

timing and patterning of Ca^{2+} action potentials generated by IHCs during a critical period before the onset of hearing are crucial for their maturation (Johnson et al., 2013a). Altered neuronal activity of the efferent input onto neonatal IHCs therefore might also affect their Ca^{2+} action potentials and hence their development.

SK2 immunolabeling was localized at the basolateral pole apart from synaptic ribbons (RIBEYE) of apical turn IHCs from 4 to 5 week-old cKO- $Ca_v1.3^{flex/-}$ and $Ca_v1.3^{-/-}$ mice (Figures 4C,D) indicating an immature phenotype. In contrast, no SK2 labeling was found at the basolateral pole of wildtype IHCs (Figure 4B).

BK channel expression was assessed in wildtype and $Ca_v1.3^{-/-}$ IHCs co-labeled with calbindin (Figures 5A–C)

and in $Ca_v1.3^{flex/-}$ controls, cKO- $Ca_v1.3^{flex/flux}$ and cKO- $Ca_v1.3^{flex/-}$ IHCs co-labeled with GFP (Figures 5D–F). BK channels, which are indicators of a mature IHC phenotype, were present at the neck of wildtype IHCs (Figure 5A). In $Ca_v1.3^{-/-}$ mice, BK labeling was absent from apical-turn IHCs (Figure 5B), whereas sparse and faint labeling was found in basal-turn IHCs (Figure 5C). In $Ca_v1.3^{flex/-}$ control IHCs, normal BK labeling was found at the neck of IHCs (Figure 5D). In true cKO IHCs i.e., IHCs with strong GFP labeling in cKO- $Ca_v1.3^{flex/flux}$ mice (Figure 5E) and with GFP labeling in cKO- $Ca_v1.3^{flex/-}$ mice (Figure 5F), BK labeling was missing. Unexpectedly, BK immunolabeling in heterozygous IHCs of both cKO genotypes, i.e., IHCs with weak (cKO- $Ca_v1.3^{flex/flux}$, Figure 5E) or no GFP labeling (cKO- $Ca_v1.3^{flex/-}$, Figure 5F), which appeared

TABLE 1 | Degeneration of IHCs in the apical and basal cochlear turn of mice with systemic (Ca_v1.3^{-/-}) and cochlea-specific deletion of Ca_v1.3 with GFP reporter function (cKO-Ca_v1.3^{flex/lex} and cKO-Ca_v1.3^{flex/-}).

	Ca _v 1.3 ^{-/-}		cKO-Ca _v 1.3 ^{flex/lex}		cKO-Ca _v 1.3 ^{flex/-}	
	Apical	Basal	Apical	Basal*	Apical	Basal
<i>n</i> ears/animals	4/3	4/3	8/4	5/4	4/4	3/3
IHCs / ear	107.3 ± 56.4	59.5 ± 29.5	156.5 ± 61.4	10.0 ± 8.2	164.8 ± 82.2	44.3 ± 38.8
Degenerated IHCs / ear	7.25 ± 5.3	0.3 ± 0.5	8.5 ± 10.2	44.8 ± 28.8	1.8 ± 1.0	0.0 ± 0.0
Degeneration (%) / ear	9.5 ± 10.2%	0.5 ± 0.9%	6.5 ± 9.1%	83.1 ± 4.7%	1.2 ± 0.7%	0.0 ± 0.0%
IHC slots, total	458	239	1320	274	666	131
IHCs, total	429	238	1252	50	659	131
Degenerated IHCs, total	29	1	68	224	7	0
Degeneration (%), total	6.3%	0.4%	6.2%	81.8%	1.1%	0%

The degree of degeneration was determined for individual ears and cochlear location (apical vs. basal) and is given as number of empty IHC slots (degenerated IHCs) per number of total IHC slots (filled + empty). Numbers per ear are given as mean ± SD. *due to profound degeneration, degenerated IHCs were determined as OHCs of the innermost OHC row minus intact IHCs.

TABLE 2 | Rate of successful *flex* switch in IHCs from the apical cochlear turn of cKO-Ca_v1.3^{flex/lex} and cKO-Ca_v1.3^{flex/-} mice at 4–6 weeks of age.

	cKO-Ca _v 1.3 ^{flex/lex}		cKO-Ca _v 1.3 ^{flex/-}	
	Mean ± SD per animal (<i>n</i> = 3)	% of IHC slots	Mean ± SD per animal (<i>n</i> = 5)	% of IHC slots
Total IHC slots (filled and empty)	285.7 ± 103.7	100.0	203.4 ± 95.2	100.0
Heterozygous IHCs	36.0 ± 36.5	12.6	22.0 ± 15.4	10.8
Knockout IHCs	207.0 ± 104.5	72.5	181.4 ± 90.5	89.2
Degenerated IHCs	42.7 ± 61.0	14.9	0.0 ± 0.0	0
cKO-IHCs	249.7 ± 67.9	87.4	181.4 ± 90.5	89.2

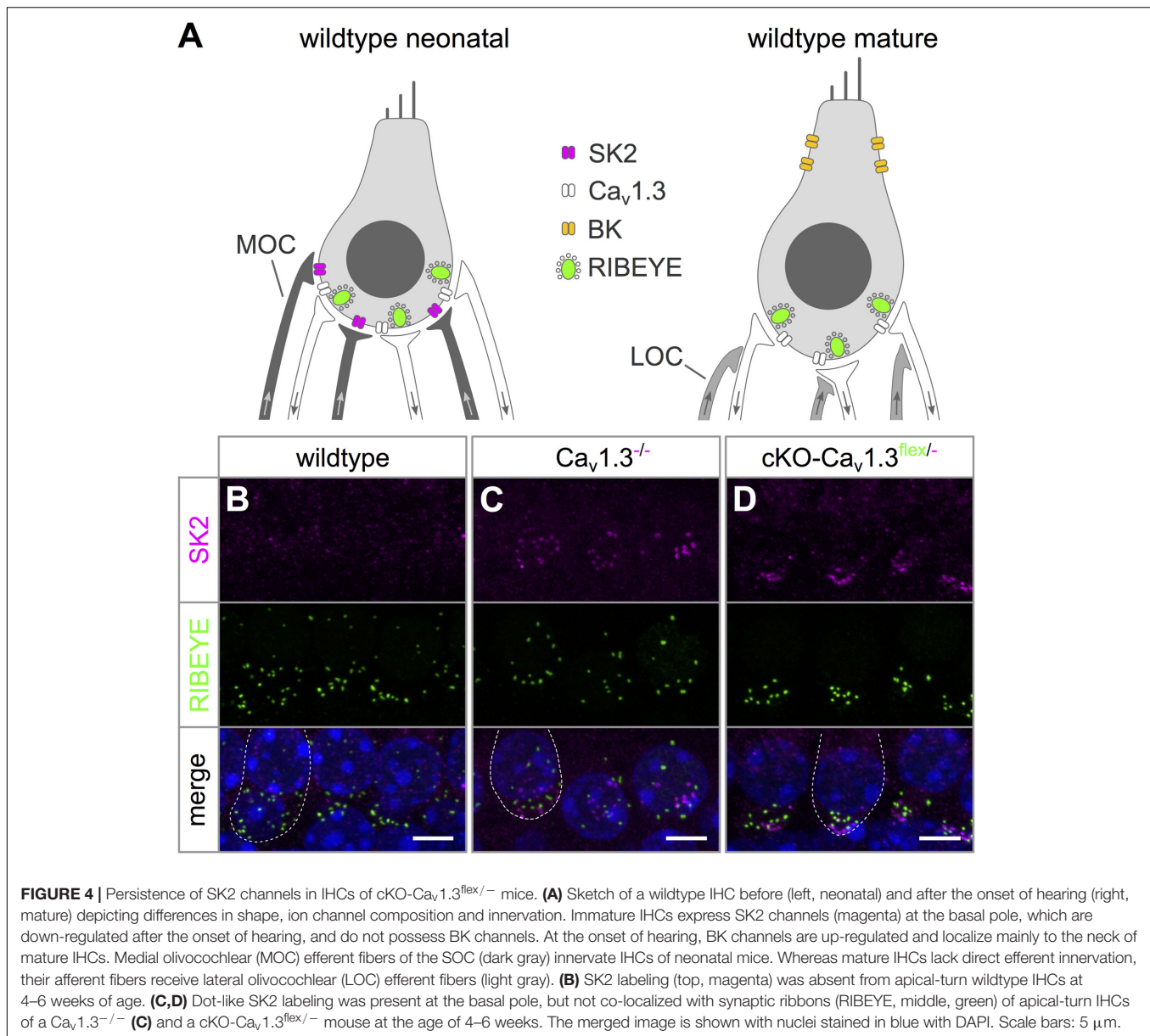
Organs of Corti labeled for Ca_v1.3, BK and/or GFP were divided in four different groups according to their phenotype: (i) knockout IHCs: lack of Ca_v1.3- or BK-positive labeling (cf. **Figures 5,6**) or strong GFP labeling in cKO-Ca_v1.3^{flex/lex} or GFP labeling in cKO-Ca_v1.3^{flex/-} mice, respectively; (ii) degenerated IHCs: empty IHC-sized slots; (iii) heterozygous IHCs: Ca_v1.3- or BK-positive labeling or weak GFP labeling in cKO-Ca_v1.3^{flex/lex} or lack of GFP labeling in cKO-Ca_v1.3^{flex/-} mice, respectively. Wildtype-like IHCs lacking GFP labeling were not found in cKO-Ca_v1.3^{flex/lex} mice. Assuming that only knockout IHCs degenerated, the percentage of IHCs with a successful deletion of Ca_v1.3 channels was calculated from the sum of knockout and degenerated IHCs (cKO-IHCs).

as small dots at the neck, clearly differed from the large BK patches in control Ca_v1.3^{flex/-} (**Figure 5D**) or wildtype IHCs (**Figure 5A**). The GFP-negative IHCs of cKO-Ca_v1.3^{flex/-} mice containing a non-switched *flex* allele should, however, have the same phenotype and thus the same BK labeling pattern as IHCs of control Ca_v1.3^{flex/-} mice.

Reduced Ba²⁺ Currents and Ca_v1.3 Protein Clusters in Control Ca_v1.3^{flex/-} IHCs

We noticed that expression of one or two *flex* alleles without Cre resulted in smaller IHC Ba²⁺ currents compared with wildtype IHCs (cf. **Figures 1D,E, 2B–E**). However, in conditional mouse lines, the function of the target gene should remain unaltered unless it is deleted or manipulated by Cre or other recombinases. For generating the conditional *Cacna1d* construct, *loxP* sites were inserted in intronic regions flanking exon 2 of the *Cacna1d* gene, which should not impair its function (Satheesh et al., 2012). To determine the side effect of the construct in the *Cacna1d-eGFP^{flex}* allele, we measured *I*_{Ba} in IHCs of mice with different combinations of wildtype (+), *flex* and knockout (–) alleles, i.e., Ca_v1.3^{+/-}, Ca_v1.3^{+/flex}, Ca_v1.3^{flex/lex} and Ca_v1.3^{flex/-} compared with wildtype mice (**Figure 6**). Averaged peak *I*_{Ba}

amplitudes of IHCs from Ca_v1.3^{flex/lex} (–102.7 ± 16.4 pA; *n* = 10) and Ca_v1.3^{flex/-} mice (–89.5 ± 17.2 pA; *n* = 10) were significantly reduced compared with wildtype (–212.4 ± 48.2 pA; *n* = 10; *P* < 0.001, Kruskal–Wallis Test; **Figure 6A**). *I*_{Ba} normalized to the wildtype (100%) was reduced to 48.4% in Ca_v1.3^{flex/lex} and 42.1% in Ca_v1.3^{flex/-} IHCs, respectively (**Figure 6B**). In mice with only one wildtype (+) allele, *I*_{Ba} was slightly but not significantly reduced to –171.6 ± 50.9 pA or 80.9% (Ca_v1.3^{+/-}; *n* = 10) and –149.5 ± 36.5 pA or 70.4% (Ca_v1.3^{+/flex}; *n* = 7; **Figures 6A,B**), respectively. In contrast, *I*_{Ba} was reduced to 5.1% in IHCs of cKO-Ca_v1.3^{flex/-} mice indicating a complete loss of Ca_v1.3 channels leaving a small residual Ca²⁺ current that has been described before in the systemic knockout (Platzer et al., 2000; Brandt et al., 2003; Dou et al., 2004). Additionally, Cre expression in the cochlea did not affect *I*_{Ba} in IHCs of *Pax2::cre* control mice (–216.4 ± 53.1 pA; *n* = 10; **Figure 6B**). Analysis of gating properties by fitting the *I–V* curves to a second-order Boltzmann function times Goldman–Hodgkin–Katz driving force yielded a small but significant shift of *V*_h by –2.5 mV in Ca_v1.3^{flex/-} (–12.6 ± 2.0 mV; *n* = 10) versus wildtype IHCs (–10.1 ± 2.3 mV; *n* = 10; *P* = 0.019, MWU test), whereas the voltage sensitivity of activation determined by the slope factor *k* was unaffected (Ca_v1.3^{flex/-}: 11.22 ± 0.97 mV; wildtype: 11.26 ± 0.30 mV; *P* = 0.762, MWU test).



In summary, reduction of I_{Ba} amplitude in IHCs of control $Ca_v1.3^{flex/flex}$ and $Ca_v1.3^{flex/-}$ mice, as well as altered gating properties in $Ca_v1.3^{flex/-}$ control IHCs demonstrate that the unswitched *Cacna1d flex* allele functionally does not fully replace the wildtype allele.

The functional reduction of $Ca_v1.3$ channels might be caused by a reduced amount of $Ca_v1.3$ channel protein in the IHC membrane or by a reduced function of $Ca_v1.3$ channels in $Ca_v1.3^{flex/-}$ mice. The abundance of $Ca_v1.3$ channel protein was assessed by co-immunolabeling for $Ca_v1.3$ (magenta) and synaptic ribbons (RIBEYE, green, **Figure 7**). $Ca_v1.3$ clusters were localized at the synaptic ribbons of wildtype IHCs (**Figure 7A,a**) and at the majority of ribbons of IHCs from $Ca_v1.3^{flex/-}$ control mice (**Figure 7C,c**). In contrast, no specific $Ca_v1.3$ labeling was found at the synapses of $Ca_v1.3^{-/-}$ IHCs (**Figure 7B,b**) and

most, but not all IHCs of cKO- $Ca_v1.3^{flex/-}$ mice (**Figure 7D,d'**). In part of the IHCs from cKO- $Ca_v1.3^{flex/-}$ mice, $Ca_v1.3$ labeling was still present at the synaptic ribbons (**Figure 7D,d''**) indicating that the *flex* allele was not switched in these cells. Synaptic ribbons (RIBEYE) of $Ca_v1.3$ -deficient IHCs from $Ca_v1.3^{-/-}$ and cKO- $Ca_v1.3^{flex/-}$ mice were agglomerated and localized closer to the nucleus (**Figures 7B,D**) as described before (Nemzou et al., 2006).

To elucidate the cause of the reduced I_{Ba} amplitude (42% of wildtype, **Figures 6A,B**) in IHCs of $Ca_v1.3^{flex/-}$ control mice, a quantitative analysis of the size and number of $Ca_v1.3$ clusters and synaptic ribbons was performed (**Figures 7E–G**). Whereas the number of $Ca_v1.3$ clusters and ribbons was unchanged, the average size of both $Ca_v1.3$ clusters and synaptic ribbons was significantly reduced to 73 and 89% in $Ca_v1.3^{flex/-}$ control IHCs

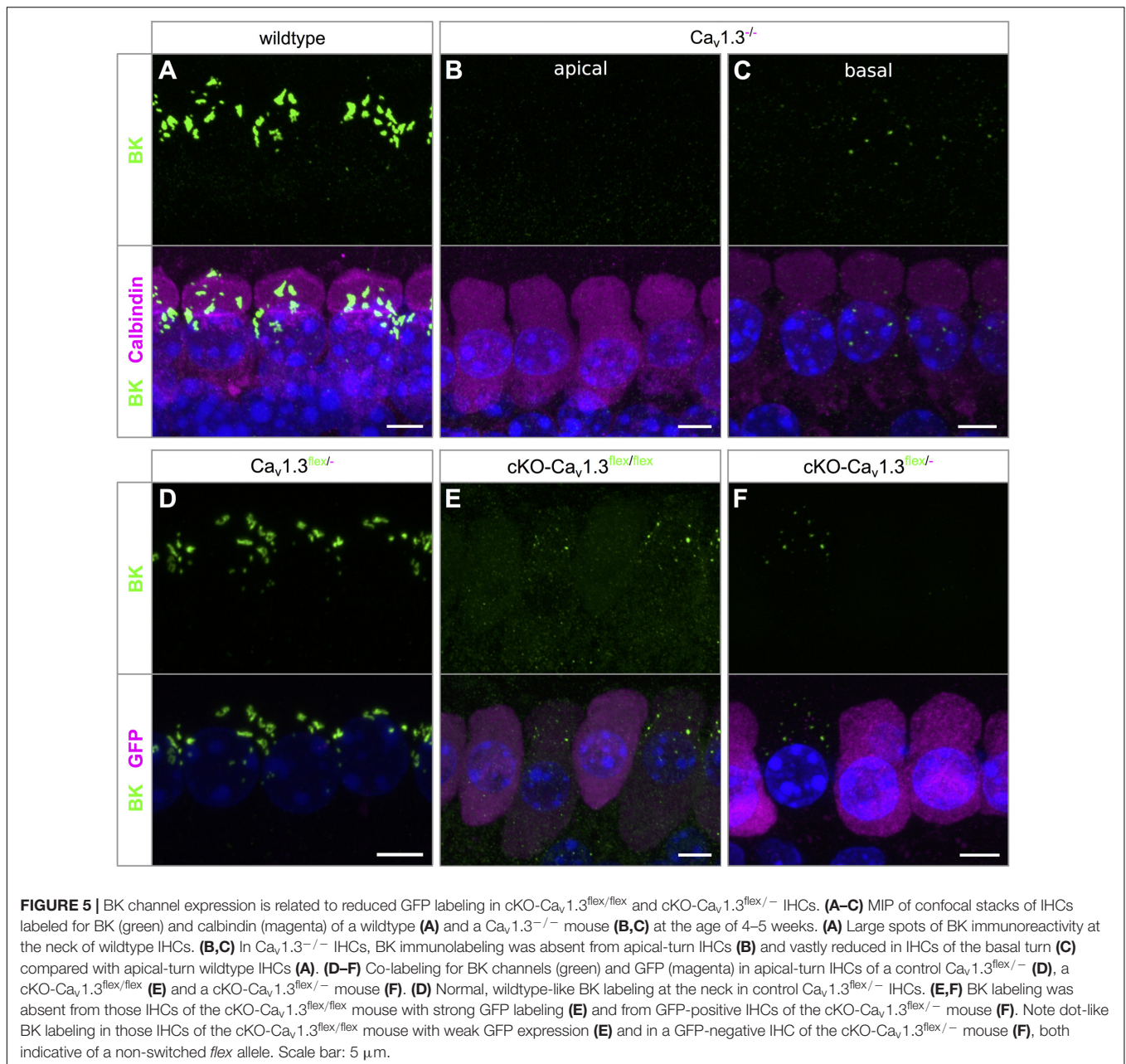


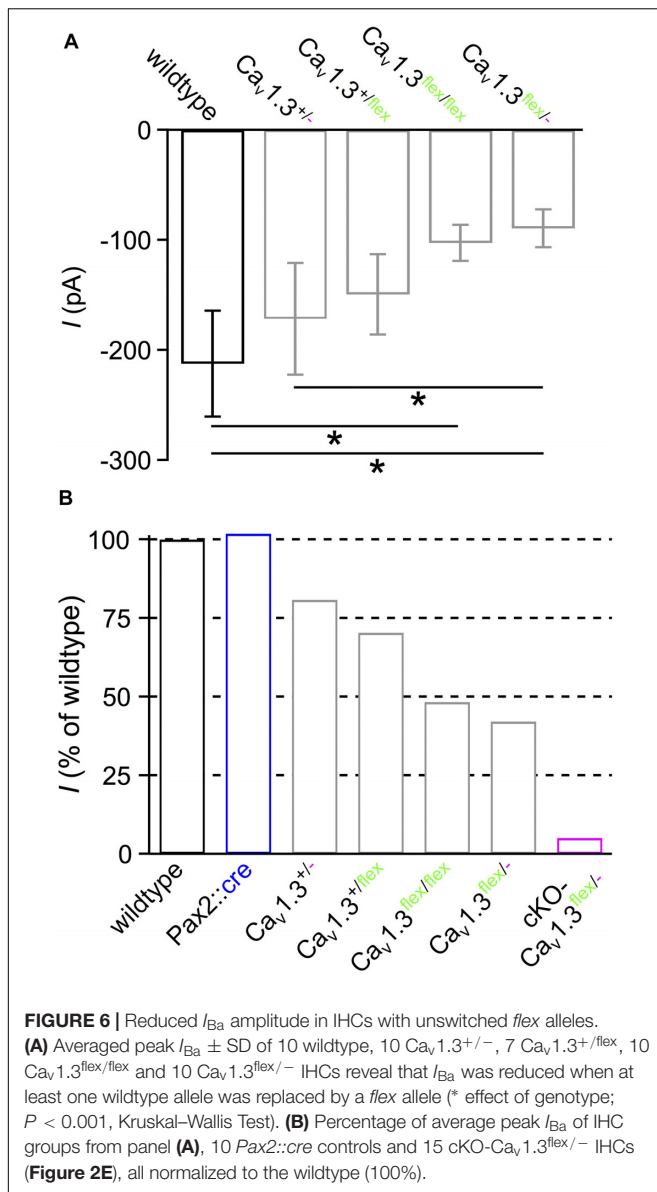
FIGURE 5 | BK channel expression is related to reduced GFP labeling in cKO- $Ca_v1.3^{flex/flex}$ and cKO- $Ca_v1.3^{flex/-}$ IHCs. **(A–C)** MIP of confocal stacks of IHCs labeled for BK (green) and calbindin (magenta) of a wildtype **(A)** and a $Ca_v1.3^{-/-}$ mouse **(B,C)** at the age of 4–5 weeks. **(A)** Large spots of BK immunoreactivity at the neck of wildtype IHCs. **(B,C)** In $Ca_v1.3^{-/-}$ IHCs, BK immunolabeling was absent from apical-turn IHCs **(B)** and vastly reduced in IHCs of the basal turn **(C)** compared with apical-turn wildtype IHCs **(A)**. **(D–F)** Co-labeling for BK channels (green) and GFP (magenta) in apical-turn IHCs of a control $Ca_v1.3^{flex/-}$ **(D)**, a cKO- $Ca_v1.3^{flex/flex}$ **(E)** and a cKO- $Ca_v1.3^{flex/-}$ mouse **(F)**. **(D)** Normal, wildtype-like BK labeling at the neck in control $Ca_v1.3^{flex/-}$ IHCs. **(E,F)** BK labeling was absent from those IHCs of the cKO- $Ca_v1.3^{flex/flex}$ mouse with strong GFP labeling **(E)** and from GFP-positive IHCs of the cKO- $Ca_v1.3^{flex/-}$ mouse **(F)**. Note dot-like BK labeling in those IHCs of the cKO- $Ca_v1.3^{flex/flex}$ mouse with weak GFP expression **(E)** and in a GFP-negative IHC of the cKO- $Ca_v1.3^{flex/-}$ mouse **(F)**, both indicative of a non-switched *flex* allele. Scale bar: 5 μ m.

compared with wildtype (**Figure 7F**). This reduction in size also applied to the total area of $Ca_v1.3$ clusters to 75% and of ribbons to 83% of the total areas in wildtype, respectively (**Figure 7G**). In conclusion, less $Ca_v1.3$ protein was produced in IHCs of $Ca_v1.3^{flex/-}$ mice evident by reduced I_{Ba} amplitudes and smaller $Ca_v1.3$ channel clusters, which was accompanied by smaller ribbons.

Profound Hearing Loss in cKO- $Ca_v1.3^{flex/-}$ and Mild Hearing Impairment in Control $Ca_v1.3^{flex/-}$ Mice

Next, we assessed how the loss/reduction of $Ca_v1.3$ channels affected the auditory function of cKO- $Ca_v1.3^{flex/-}$ and control

mice. In 4–6 week-old cKO- $Ca_v1.3^{flex/-}$ mice, click-evoked ABR thresholds (**Figure 8A**) were absent (threshold > 100 dB SPL) in 4/3 ears/animals and significantly elevated in the remaining 12/7 out of 16/8 ears/animals (81.3 ± 8.0 dB SPL; $P < 0.001$) compared with wildtype mice (17.9 ± 6.7 dB SPL, 14/7 ears/animals). In contrast, click ABR thresholds were unaffected in all control groups (*Pax2::cre*: 13.8 ± 7.6 dB SPL, 16/8 ears/animals; $Ca_v1.3^{+/flex}$: 16.3 ± 4.3 dB SPL, 12/6 ears/animals; $Ca_v1.3^{flex/-}$: 20.4 ± 4.1 dB SPL, 14/7 ears/animals; $P > 0.05$; one-way ANOVA with Bonferroni *post hoc* test, **Figure 8A**). Frequency-dependent ABR (f-ABR) thresholds (**Figure 8B**) could only be measured in part of the cKO- $Ca_v1.3^{flex/-}$ mice analyzed (16/8 ears/animals, single data points)



and were thus not included in the statistical analysis. f-ABR thresholds of *Pax2::cre* (15/8 ears/animals) and $Ca_v1.3^{flex/-}$ (14/7 ears/animals) significantly differed from wildtype mice (14/7 ears/animals; two-way ANOVA with Bonferroni *post hoc* test, effect of genotype: $P < 0.001$). Specifically, thresholds were increased in $Ca_v1.3^{flex/-}$ control mice ($P < 0.001$), reaching significance at all frequencies except at 22.6 kHz; and slightly reduced in *Pax2::cre* mice ($P = 0.001$), reaching significance at 2 and 8 kHz.

Averaged ABR waveforms of $Ca_v1.3^{flex/-}$ controls had smaller amplitudes than in wildtype mice for click stimuli 40 dB above threshold (**Figure 8C**). Growth functions of peak-to-peak amplitudes showed a significant reduction of all waves in $Ca_v1.3^{flex/-}$ control (14/7 ears/animals) compared with wildtype (wave I, IV: 14/7 ears/animals; wave II, III: 12/6 ears/animals,

Figure 8D), revealed by a regression analysis of the smaller slopes of fits to the amplitudes as a function of level above threshold of wave I to IV (wave I, $P < 0.001$; wave II, $P = 0.015$; wave III, $P < 0.001$; wave IV, $P = 0.027$; *MWU* test) and a smaller *y*-axis intercept value of wave I (*MWU* test, $P = 0.002$). Growth functions of latencies, calculated as time between stimulus application and the negative peak of the respective wave, were not significantly altered for all waves (I – IV) in $Ca_v1.3^{flex/-}$ control mice compared with the wildtype (**Figure 8E**).

Finally, we tested the function of the cochlear amplifier including OHC electromotility by measuring DPOAEs (**Figure 8F**). Mean 2f₁–f₂ DPOAE maximum amplitudes averaged between 10 and 18 kHz in 0.5 kHz steps were strongly reduced in cKO- $Ca_v1.3^{flex/-}$ mice (12/7 ears/animals, $P < 0.001$, Kruskal–Wallis Test, effect of genotype) but unaffected in all control groups (wildtype: 14/7 ears/animals; *Pax2::cre*: 16/8 ears/animals; $Ca_v1.3^{+flex}$: 12/6 ears/animals; $Ca_v1.3^{flex/-}$: 14/7 ears/animals).

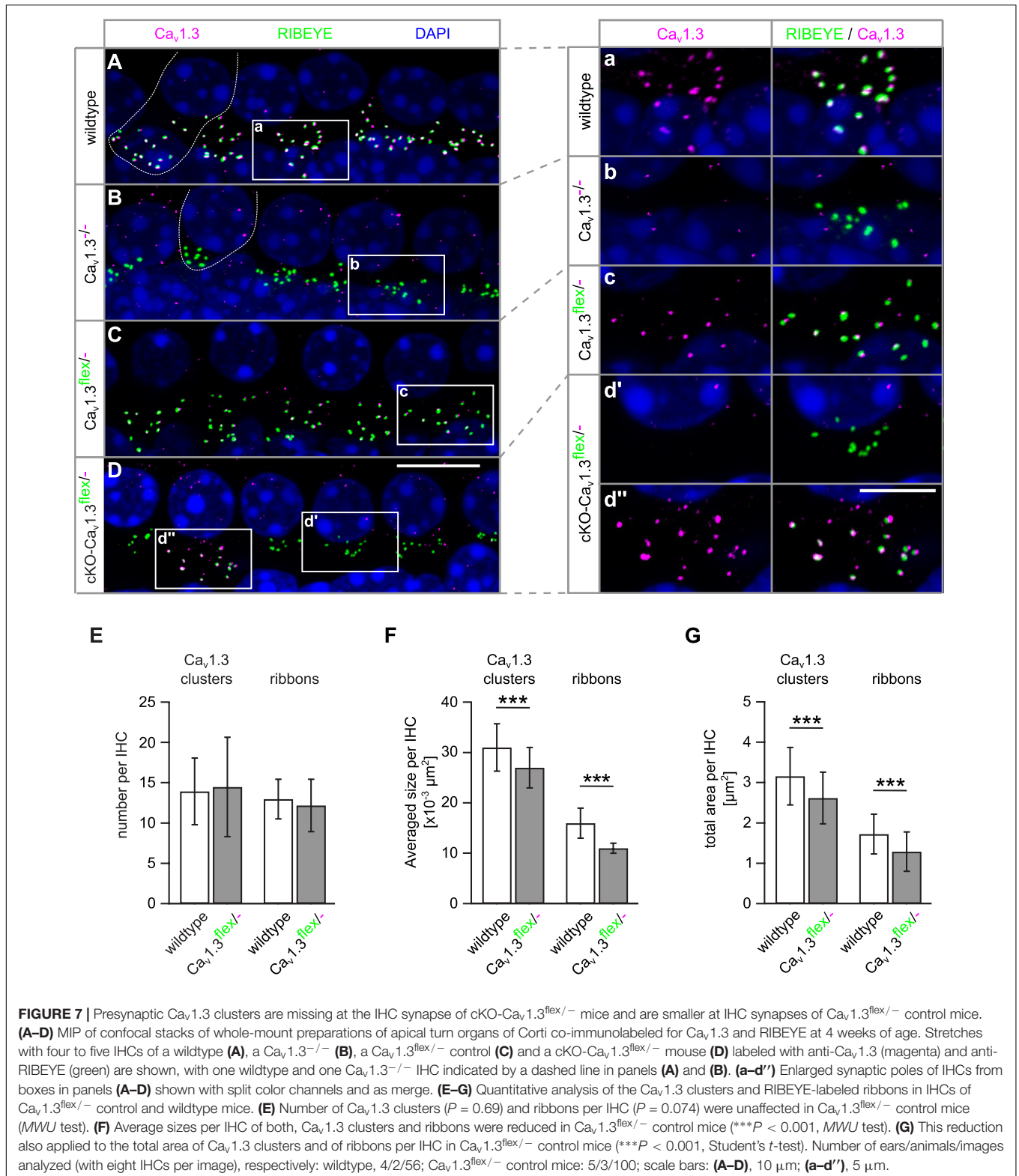
In summary, cochlea-specific deletion of $Ca_v1.3$ in cKO- $Ca_v1.3^{flex/-}$ mice resulted in highly elevated ABR thresholds and strongly reduced DPOAEs, reflecting profound hearing loss. Moreover, in $Ca_v1.3^{flex/-}$ control mice the reduction of mean IHC I_{Ba} amplitude to 42% and of mean $Ca_v1.3$ cluster size to 73% is accompanied by increases in f-ABR thresholds up to 10–20 dB and strongly reduced amplitudes of ABR waves I to IV. Notably, click-ABR thresholds and DPOAEs were not affected in $Ca_v1.3^{flex/-}$ control mice.

DISCUSSION

Here we show that cochlea-specific ablation of $Ca_v1.3$ channels resulted in an IHC phenotype replicating that of systemic $Ca_v1.3^{-/-}$ mice. For obtaining a cochlea-specific $Ca_v1.3$ knockout mouse, we started with a conditional $Ca_v1.3^{flex/flex}$ mouse model that was crossed with a cochlea-specific Cre line, *Pax2::cre*. When determining Ca^{2+} channel currents through $Ca_v1.3$ channels we found inefficient switch of both *flex* alleles in mice aged 3 weeks. In addition, IHCs of the basal cochlear turn from cKO- $Ca_v1.3^{flex/flex}$ mice were largely degenerated at 4–6 weeks of age, but not in cKO- $Ca_v1.3^{flex/-}$ mice. Moreover, it turned out that the *flex* allele itself had an impact on $Ca_v1.3$ expression in IHCs. These obstacles demanded an in-depth analysis of the problems of the conditional mouse models used before drawing conclusions on the auditory phenotype caused by cochlea-specific deletion of $Ca_v1.3$.

Conditional Tissue-Specific Knockout Mice – Benefits and Pitfalls

Satheesh et al. (2012) were the first to analyze a conditional $Ca_v1.3$ knockout mouse model with deletion in the auditory brainstem, the *Egr2::cre;Cacna1d-eGFP^{flex/flex}* mouse. There, eGFP fluorescence was not detectable in unfixed brain tissue (Bartels, 2009), most likely due to the much lower abundance of eGFP/ $Ca_v1.3$ in these brainstem nuclei compared with IHCs. In the present study, the *flex* allele had the advantage



that successful deletion of Ca_v1.3 in IHCs resulted in eGFP fluorescence that could be judged semi-quantitatively at the cellular level. Moreover, the presence of individual IHCs where

the *flex* allele was not switched enabled us to use these cells as positive controls, e.g., for Ca_v1.3 immunolabeling within one specimen.

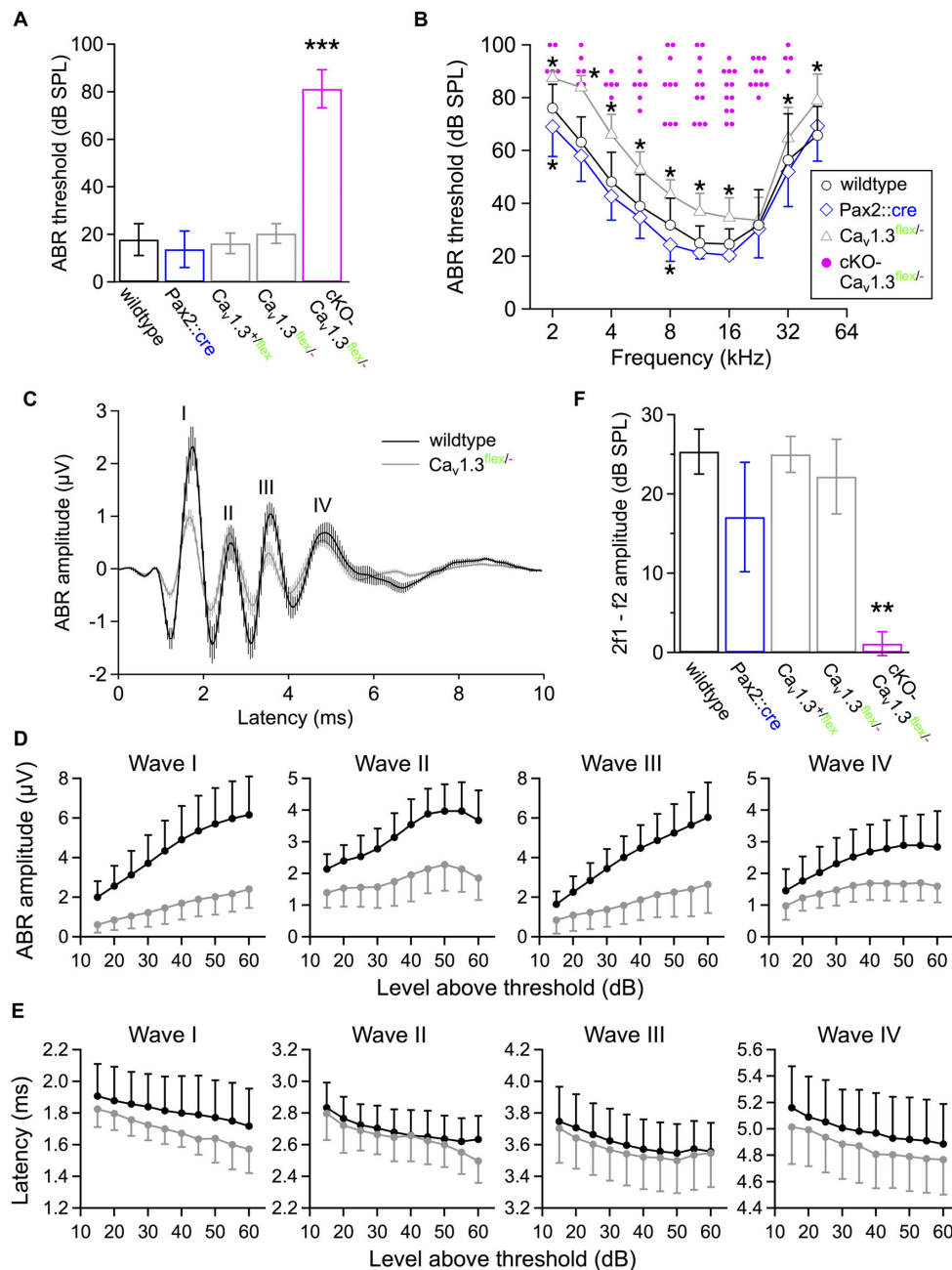


FIGURE 8 | Hearing function of 4–6 week-old cKO-Ca_v1.3^{flex/-} and control mice assessed by measurements of auditory brainstem responses (ABR) and distortion product otoacoustic emissions (DPOAE). **(A)** Click-evoked ABR thresholds (mean ± SD) were measured when ≤100 dB SPL in 12/7 out of 16/8 ears/animals of cKO-Ca_v1.3^{flex/-} mice. They were significantly increased compared with wildtype (14/7 ears/animals) and controls (*Pax2::cre*, 16/8 ears/animals; Ca_v1.3^{+/flex}, 12/6 ears/animals; Ca_v1.3^{flex/-}, 14/7 ears/animals, ****P* < 0.001, one-way ANOVA with Bonferroni *post hoc* test). **(B)** Frequency-specific ABR thresholds of cKO-Ca_v1.3^{flex/-} mice (single data, pink) could be determined in ears/animals: 2 kHz, 5/3; 2.8 kHz, 6/3; 4 kHz, 6/3; 5.6 kHz, 7/4; 8 kHz, 10/5; 11.3 kHz, 12/7; 16 kHz, 12/6; 22.6 kHz, 10/6; 32 kHz, 4/4; 45.2 kHz, 0/0; out of a total of 16/8 ears/animals recorded. Frequency-dependent ABR thresholds were increased in Ca_v1.3^{flex/-} control mice (14/7 ears/animals; group effect of two-way ANOVA with Bonferroni *post hoc* test, *P* < 0.001; effect of genotype at 2, 2.8, 4, 5.6, 8, 11.3, 16, 32 and 45.2 kHz) and reduced in *Pax2::cre* control mice (15/8 ears/animals; group effect of two-way ANOVA with Bonferroni *post hoc* test, *P* < 0.001; * effect of genotype at 2 and 8 kHz) compared with wildtype (14/7 ears/animals). **(C)** Averaged ABR waveforms to click stimuli at 40 dB above threshold (mean ± SEM) for cKO-Ca_v1.3^{flex/-} mice (single data, pink) and 14/7 Ca_v1.3^{flex/+} control ears/animals (gray). **(D)** Mean DPOAE maximum amplitudes ± SD with f1 starting at 10.0 kHz, L1 = 55 dB SPL, f2 = 1.2 × f1 averaged over 10–18 kHz in 0.5 kHz steps, and L2 = 45 dB SPL were reduced in cKO-Ca_v1.3^{flex/-} mice (14/7 ears/animals) compared with wildtype (14/7 ears/animals) and controls (*Pax2::cre*, 16/8 ears/animals; Ca_v1.3^{+/flex}, 12/6 ears/animals; Ca_v1.3^{flex/-}, 14/7 ears/animals; Kruskal–Wallis with Bonferroni *post hoc* test, ***P* ≤ 0.008). **(E,F)** Growth functions of amplitudes and latencies of waves I to IV (mean ± SD) revealed reduced mean amplitude values for all four waves and all stimulus levels in Ca_v1.3^{flex/-} control (gray; *n* = 14/7 ears/animal) compared with wildtype mice (black; *n* = 12–14/6–7 ears/animals). For clarity, the SD is plotted in one direction only (+SD or -SD).

An unwanted side effect of transgenic animals is unexpected germline expression of Cre recombinase resulting in embryonal recombination of *loxP* sites that might even occur in Cre-negative offspring carrying a *flex* or *lox* allele (Song and Palmiter, 2018). This can be monitored (i) by adapting the genotyping protocol to recognize excised or switched *lox* or *flex* alleles and (ii) in the *flex* switch system as eGFP expression in cells of Cre-negative *flex* control mice with one or two *flex* alleles.

Without the GFP reporter function, we might not have detected the incomplete recombination of *flex* alleles in IHCs. Partial recombination of floxed alleles, resulting in a mixture of cells with recombination of both, one or even no allele, is a frequent problem in conditional knockout mice (Saam and Gordon, 1999; Schulz et al., 2007; Weis et al., 2010). Lack of knowledge about the amount of successful cellular deletion events may lead to wrong conclusions caused by residual functions contributed by non-knockout cells. In this study, about 10% of the IHCs in cKO-Ca_v1.3^{flex/-} mice carried an unswitched *flex* allele resulting in residual hearing function compared with complete deafness of Ca_v1.3^{-/-} mice (Platzer et al., 2000; Dou et al., 2004).

Our attempt to increase the success rate of Cre in switching the *flex* alleles by replacing one *flex* by a constitutive knockout (“-”) allele resulted in a higher ratio of true knockout IHCs in cKO-Ca_v1.3^{flex/-} compared with cKO-Ca_v1.3^{flex/flex} mice (cf. **Figures 1, 2**) at 3 weeks of age. However, this difference was no longer present 2 weeks later (**Table 2**), indicating that Cre managed to switch most *flex* alleles by this time point. An alternative approach to increase the recombination rate of *loxP* sites would be to increase expression of Cre recombinase (Schnütgen et al., 2003; Schulz et al., 2007) using *Pax2::cre/cre* instead of *Pax2::cre/+* mice. However, high Cre expression levels on the other hand might increase the risk of possible side effects. High levels of Cre expression in α -myosin heavy chain-Cre mice have for example been demonstrated to be cardiotoxic causing altered cardiac function, DNA damage and inflammation (Bhandary and Robbins, 2015; Pugach et al., 2015). A dose dependence of Cre toxicity has been confirmed in cell culture titration experiments (Loonstra et al., 2001; Baba et al., 2005).

In summary, due to ambiguous eGFP expression in cKO-Ca_v1.3^{flex/flex} mice when only one *flex* allele was switched resulting in heterozygous IHCs that still produced Ca_v1.3, we decided to further use cKO-Ca_v1.3^{flex/-} mice, where eGFP expression was a reliable marker of Ca_v1.3 ablation. Since incomplete recombination of both *flex* (or *lox*) alleles is likely to be a general problem in conditional mice, a combination with a systemic knockout allele (*flex/-* or *lox/-*) should be used if possible.

Toxicity of Excessive eGFP

Degeneration of IHCs in the basal cochlear turn as early as P25 in cKO-Ca_v1.3^{flex/flex} but not Ca_v1.3^{-/-} mice suggests toxicity of excessive eGFP. Furthermore, direct fluorescence

of eGFP can be seen in non-fixed IHCs (this study) but not in the auditory brainstem (Bartels, 2009), further indicating particularly high expression of Ca_v1.3 in wildtype and eGFP in cKO-Ca_v1.3^{flex/flex} IHCs, respectively. GFP toxicity has been demonstrated in cell lines where its expression induced apoptosis (Liu et al., 1999) or inhibited polyubiquitination (Baens et al., 2006). In mice, neuronal expression of yellow fluorescent protein induced multiple dose-dependent stress responses (Comley et al., 2011). A possible cause for these damaging effects is that the pre-mature, colorless form of eGFP, which is present in variable proportions in GFP-expressing cells, produces the free radical O₂^{•-} and hydrogen peroxide (H₂O₂) under consumption of NAD(P)H (Ganini et al., 2017). Such a GFP-induced oxidative stress may explain why only IHCs of cKO-Ca_v1.3^{flex/flex} mice but not of cKO-Ca_v1.3^{flex/-} degenerated because of the higher dose of eGFP produced by two *flex* alleles.

Side Effects of Gene-Targeted Alleles Without Gene Deletion by Cre Recombinase

In conditional models, the modifications of the target gene should not affect its function unless recombined by Cre. In the study of Satheesh et al. (2012), who first described the Ca_v1.3-*flex* model, Ca²⁺ currents were not analyzed. Normal ABR thresholds of Ca_v1.3^{flex/flex} control mice led the authors to the conclusion that unswitched *flex* alleles did not affect Ca_v1.3 channel function. Since Ca_v1.3 channels mediate the majority of Ca²⁺ current in IHCs, the present study provided the unique opportunity to analyze potential side effects of the *flex* construct in detail by measuring Ca²⁺ channel currents and quantitatively analyzing Ca_v1.3 protein clusters. We found reduced *I*_{Ba} amplitudes and a lower amount of Ca_v1.3 protein in IHCs of cre-negative Ca_v1.3^{flex/flex} and Ca_v1.3^{flex/-} control mice demonstrating that the unswitched *flex* allele did not fully replace the wildtype function. As has been shown before, a considerable reduction or increase in peak Ca²⁺ current amplitudes of IHCs has only minor effects on click ABR thresholds (Scharinger et al., 2015; Fell et al., 2016), which can be misleading when used as the only method to assess the function of IHCs. Here, frequency-dependent ABR thresholds were increased by 10–20 dB at most frequencies in Ca_v1.3^{flex/-} control mice upon reduction of *I*_{Ba} to 42% of the wildtype value, which is in accordance to threshold increases of 5–20 dB in null mutants of the auxiliary $\alpha_2\delta_2$ Ca²⁺ channel subunit causing reductions of *I*_{Ba} to 60–70% (Fell et al., 2016). The most prominent consequence of *I*_{Ba} reduction with respect to hearing function of Ca_v1.3^{flex/-} control mice are the reduced growth functions of peak-to-peak amplitudes of the ABR waves, especially wave I, indicating strongly reduced IHC output at all levels above threshold. It should be kept in mind that both click and frequency-specific ABR thresholds are determined by only one afferent fiber type, the low threshold, high spontaneous rate fibers, whereas growth functions of ABR amplitudes cover the activity of all (high, medium and low spontaneous rate) afferent fiber types (Kiang

et al., 1965; Liberman, 1978, 1982; Petitpré et al., 2018; Shrestha et al., 2018; Sun et al., 2018).

The question arises as to why I_{Ba} was reduced in IHCs of Cre-negative mice containing at least one *flex* allele (Figure 6). For generating the conditional Ca_v1.3 mouse, the *Cacna1d-eGFP^{flex}* construct was placed outside and a few hundred base pairs up- and downstream of the coding regions of exon 2 in the *Cacna1d* gene to avoid unintended manipulation of regulatory elements flanking the exon (Bartels, 2009). This insertion might have disrupted unknown regulatory elements and thus reduced the expression level of the channel. Moreover, I_{Ba} gating properties were altered in Ca_v1.3^{flex/-} control mice, suggesting that insertion of the *flex* construct might have affected splicing of *Cacna1d* mRNA (Bock et al., 2011; Scharinger et al., 2015).

The IHC and Auditory Phenotype Following Systemic Versus Cochlea-Specific Deletion of Ca_v1.3 Channels

The ablation of Ca_v1.3 channels before birth in cKO-Ca_v1.3^{flex/-} mice caused an IHC phenotype similar to that of Ca_v1.3^{-/-} mice, including persistent expression of SK2, lack of BK expression in apical-turn IHCs, and a reduced cell size (Brandt et al., 2003; Glueckert et al., 2003; Nemzou et al., 2006).

Until the onset of hearing, SK2 channels mediate efferent inhibition of IHCs via $\alpha 9\alpha 10$ Ca²⁺-permeable nicotinic acetylcholine receptors (nAChRs) (Oliver et al., 2000; Elgoyhen et al., 2001). The origin of these efferent fibers lies in cholinergic neurons in the SOC. Shortly after birth, neurons of the auditory brainstem are spontaneously active and undergo a developmental program including synaptic pruning and establishment of tonotopy (Blankenship and Feller, 2010; Clause et al., 2014). The spiking pattern of SOC neurons is modulated by ascending information from the cochlea, where IHCs produce spontaneous Ca²⁺ action potentials, which are synchronized by Ca²⁺ waves in the transient Kölliker's organ (Tritsch and Bergles, 2010; Johnson et al., 2011, 2017; Sendin et al., 2014; Eckrich et al., 2018; Mammano and Bortolozzi, 2018). In turn, efferent inhibition from the SOC closes a feedback loop by shaping the spontaneous activity of IHCs (Guinan, 2006; Frank and Goodrich, 2018). In the systemic Ca_v1.3 knockout mouse both SOC neurons and IHCs lack Ca_v1.3 currents (Platzer et al., 2000; Hirtz et al., 2011), the latter of which as a consequence cannot produce action potentials (Brandt et al., 2003). In the SOC of Ca_v1.3^{-/-} mice, depolarization-induced spiking of lateral superior olive (LSO) neurons was changed from a single to a multiple firing pattern due to a reduction in K_v1.2 channels (Hirtz et al., 2011). This was most likely caused by the specific lack of Ca_v1.3 channels in brainstem neurons despite intact cochlear expression as confirmed in brainstem-specific Ca_v1.3 knockout mice (Satheesh et al., 2012). In the present study with SOC neurons expressing Ca_v1.3 channels, the phenotype of Ca_v1.3-deficient IHCs from cKO-Ca_v1.3^{flex/-} mice (lack of BK channels, persistence of SK2 channels, smaller

cell size) was very similar to that of systemic Ca_v1.3^{-/-} mice. Therefore a potentially altered feedback signaling by Ca_v1.3-deficient SOC neurons onto IHCs cannot be causative for the IHC phenotype of Ca_v1.3^{-/-} mice. Nevertheless, the spiking pattern of SOC neurons and, thus, efferent signaling back to immature IHCs might still be altered due to the loss of afferent activation by IHCs. In $\alpha 9$ - and $\alpha 10$ -nAChR knockout mice, maturation of IHC K⁺ channels was normal despite the complete lack of cholinergic efferent input from SOC neurons (Gomez-Casati et al., 2009; Johnson et al., 2013b). In summary, maturation of the IHC's K⁺ channel composition is mainly controlled by intrinsic Ca²⁺ signaling within the IHC and does not depend on Ca_v1.3 expression in the SOC exerting efferent feedback.

BK Channel Expression in Basal-Turn IHCs of Ca_v1.3^{-/-} and Cre-Negative IHCs of cKO-Ca_v1.3^{flex/-} Mice

We found residual BK labeling in IHCs of the basal but not the apical cochlear turn of Ca_v1.3^{-/-} mice. So far it is unknown why BK protein is missing in IHCs of Ca_v1.3^{-/-} mice along most of the cochlear length (Brandt et al., 2003) despite expression of the respective *Kcnma1* mRNA (Nemzou et al., 2006).

The faint and dot-like BK labeling in GFP-negative IHCs of cKO-Ca_v1.3^{flex/-} mice clearly differed from the large BK patches found in IHCs of wildtype and control Ca_v1.3^{flex/-} mice (Figure 5F). Assuming that Cre is not active in these IHCs their phenotype should be the same as that of Ca_v1.3^{flex/-} controls (Figure 5D) but this was not the case. We can thus exclude that the reduced BK expression was caused by the incomplete wildtype function of the unswitched *flex* allele. But what are the differences between IHCs of Ca_v1.3^{flex/-} controls and GFP-negative IHCs of cKO-Ca_v1.3^{flex/-} mice? Differences intrinsic to the IHCs are: (i) Presence of the *Pax2::cre* allele at an unknown location in the genome, which might interfere with modulatory sequences affecting BK expression; (ii) Cre might be expressed in these IHCs without switching the *flex* allele, but it could still interfere with BK expression. Alternatively, a factor extrinsic to the IHC might be causing the reduced BK expression. GFP-negative IHCs of cKO-Ca_v1.3^{flex/-} mice are surrounded by Ca_v1.3-deficient, electrically silent IHCs, whereas neonatal IHCs produce Ca²⁺ action potentials in wildtype and presumably Ca_v1.3^{flex/-} mice (Brandt et al., 2003). This activity causes periodic efflux of K⁺ ions from the IHCs, which depolarizes neighboring phalangeal cells and IHCs, thereby amplifying and synchronizing Ca²⁺ AP activity (Wang et al., 2015; Eckrich et al., 2018). In summary, impaired expression of BK channels in solitary GFP-negative IHCs surrounded by true Ca_v1.3 knockout IHCs of cKO-Ca_v1.3^{flex/-} mice may result from a lack of mutual activation and synchronization of Ca²⁺ AP activity among IHCs during the critical developmental period. It would be interesting to analyze whether the Ca²⁺ action potential activity in GFP-negative IHCs of cKO-Ca_v1.3^{flex/-} is altered compared to Ca_v1.3^{flex/-} controls.

DATA AVAILABILITY

The datasets generated for this study are available on request to the corresponding author.

ETHICS STATEMENT

All experiments were carried out in accordance with the European Communities Council Directive (86/609/EEC) and approved by the regional board for scientific animal experiments of the Saarland, Germany. Additional ethics approval was not required according to the local and national guidelines.

AUTHOR CONTRIBUTIONS

SE and JE conceived and designed the study. SE, DH, KS, KB, KF, and SM acquired the data. SE, JE, DH, KB, SM,

GW, and BS drafted the article. JE contributed to funding acquisition and project administration. All authors analyzed and interpreted the data.

FUNDING

This work was supported by DFG SFB 894 (A8 to JE), EU-CAVNET MRTN-CT-2006-035367 (to JE), DFG Priority Program 1608 “Ultrafast and Temporally Precise Information Processing: Normal and Dysfunctional Hearing” (En 294/5-2 to JE), DFG EC 488/1-1 (to SE), and Saarland University.

ACKNOWLEDGMENTS

We thank Jennifer Ihl, Angela Di Turi, and Barbara Fell for excellent technical assistance and Kai Schöning and Dušan Bartsch for discussion of the data.

REFERENCES

- Baba, Y., Nakano, M., Yamada, Y., Saito, I., and Kanegae, Y. (2005). Practical range of effective dose for cre recombinase-expressing recombinant adenovirus without cell toxicity in mammalian cells. *Microbiol. Immunol.* 49, 559–570. doi: 10.1111/j.1348-0421.2005.tb03753.x
- Babola, T. A., Li, S., Gribizis, A., Lee, B. J., Issa, J. B., Wang, H. C., et al. (2018). Homeostatic control of spontaneous activity in the developing auditory system. *Neuron* 99, 511.e5–524.e5. doi: 10.1016/j.neuron.2018.07.004
- Baens, M., Noels, H., Broeckx, V., Hagens, S., Fevery, S., Billiau, A. D., et al. (2006). The dark side of EGFP: defective polyubiquitination. *PLoS One* 1:e54. doi: 10.1371/journal.pone.0000054
- Baig, S. M., Koschak, A., Lieb, A., Gebhart, M., Dafinger, C., Nürnberg, G., et al. (2011). Loss of Cav1.3 (CACNA1D) function in a human channelopathy with bradycardia and congenital deafness. *Nat. Neurosci.* 14, 77–84. doi: 10.1038/nn.2694
- Bartels, K. (2009). *Conditional Knockout of the L-Type Voltage-Gated Calcium Channel CaV1.3 via the FLEX Switch*. Thesis. Heidelberg: Ruprecht-Karls-Universität Heidelberg, doi: 10.11588/heidok.00010021
- Bhandary, B., and Robbins, J. (2015). Giving credence to controls: avoiding the false phenotype. *J. Mol. Cell. Cardiol.* 86, 136–137. doi: 10.1016/j.yjmcc.2015.07.007
- Blankenship, A. G., and Feller, M. B. (2010). Mechanisms underlying spontaneous patterned activity in developing neural circuits. *Nat. Rev. Neurosci.* 11, 18–29. doi: 10.1038/nrn2759
- Bock, G., Gebhart, M., Scharinger, A., Jangsongthong, W., Busquet, P., Poggiani, C., et al. (2011). Functional properties of a newly identified c-terminal splice variant of Cav1.3 L-type Ca²⁺ channels. *J. Biol. Chem.* 286, 42736–42748. doi: 10.1074/jbc.M111.269951
- Brandt, A., Striessnig, J., and Moser, T. (2003). CaV1.3 channels are essential for development and presynaptic activity of cochlear inner hair cells. *J. Neurosci.* 23, 10832–10840. doi: 10.1523/JNEUROSCI.23-34-10832.2003
- Burton, Q., Cole, L. K., Mulheisen, M., Chang, W., and Wu, D. K. (2004). The role of Pax2 in mouse inner ear development. *Dev. Biol.* 272, 161–175. doi: 10.1016/j.ydbio.2004.04.024
- Clause, A., Kim, G., Sonntag, M., Weisz, C. J. C., Vetter, D. E., Rübsamen, R., et al. (2014). The precise temporal pattern of prehearing spontaneous activity is necessary for tonotopic map refinement. *Neuron* 82, 822–835. doi: 10.1016/j.neuron.2014.04.001
- Comley, L. H., Wishart, T. M., Baxter, B., Murray, L. M., Nimmo, A., Thomson, D., et al. (2011). Induction of cell stress in neurons from transgenic mice expressing yellow fluorescent protein: implications for neurodegeneration research. *PLoS One* 6:e17639. doi: 10.1371/journal.pone.0017639
- Dou, H., Vazquez, A. E., Namkung, Y., Chu, H., Cardell, E. L., Nie, L., et al. (2004). Null mutation of alpha1D Ca²⁺ channel gene results in deafness but no vestibular defect in mice. *J. Assoc. Res. Otolaryngol.* 5, 215–226. doi: 10.1007/s10162-003-4020-3
- Eckrich, T., Blum, K., Milenkovic, I., and Engel, J. (2018). Fast Ca²⁺ transients of inner hair cells arise coupled and uncoupled to Ca²⁺ waves of inner supporting cells in the developing mouse cochlea. *Front. Mol. Neurosci.* 11:264. doi: 10.3389/fnmol.2018.00264
- Elgoyhen, A. B., Vetter, D. E., Katz, E., Rothlin, C. V., Heinemann, S. F., and Boulter, J. (2001). $\alpha 10$: a determinant of nicotinic cholinergic receptor function in mammalian vestibular and cochlear mechanosensory hair cells. *Proc. Natl. Acad. Sci. U.S.A.* 98, 3501–3506. doi: 10.1073/pnas.051622798
- Engel, J., Braig, C., Ruttiger, L., Kuhn, S., Zimmermann, U., Blin, N., et al. (2006). Two classes of outer hair cells along the tonotopic axis of the cochlea. *Neuroscience* 143, 837–849. doi: 10.1016/j.neuroscience.2006.08.060
- Fell, B., Eckrich, S., Blum, K., Eckrich, T., Hecker, D., Obermair, G. J., et al. (2016). $\alpha 282$ controls the function and trans-synaptic coupling of Cav1.3 channels in mouse inner hair cells and is essential for normal hearing. *J. Neurosci.* 36, 11024–11036. doi: 10.1523/JNEUROSCI.3468-14.2016
- Frank, M. M., and Goodrich, L. V. (2018). Talking back: development of the olivocochlear efferent system. *Wiley Interdiscip. Rev. Dev. Biol.* 7:e324. doi: 10.1002/wdev.324
- Ganini, D., Leinisch, F., Kumar, A., Jiang, J., Tokar, E. J., Malone, C. C., et al. (2017). Fluorescent proteins such as eGFP lead to catalytic oxidative stress in cells. *Redox Biol.* 12, 462–468. doi: 10.1016/j.redox.2017.03.002
- Glowatzki, E., and Fuchs, P. A. (2000). Cholinergic synaptic inhibition of inner hair cells in the neonatal mammalian cochlea. *Science* 288, 2366–2368. doi: 10.1126/science.288.5475.2366
- Glueckert, R., Wietzorrek, G., Kammen-Jolly, K., Scholtz, A., Stephan, K., Striessnig, J., et al. (2003). Role of class D L-type Ca²⁺ channels for cochlear morphology. *Hear. Res.* 178, 95–105. doi: 10.1016/S0378-5955(03)00054-6
- Gomez-Casati, M. E., Wedemeyer, C., Taranda, J., Lipovsek, M., Dalamon, V., Elgoyhen, A. B., et al. (2009). Electrical properties and functional expression of ionic channels in cochlear inner hair cells of mice lacking the alpha10 nicotinic cholinergic receptor subunit. *J. Assoc. Res. Otolaryngol.* 10, 221–232. doi: 10.1007/s10162-009-0164-0

- Guinan, J. J. (2006). Olivocochlear efferents: anatomy, physiology, function, and the measurement of efferent effects in humans. *Ear Hear.* 27, 589–607. doi: 10.1097/01.aud.0000240507.83072.e7
- Hirtz, J. J., Boesen, M., Braun, N., Deitmer, J. W., Kramer, F., Lohr, C., et al. (2011). Cav1.3 calcium channels are required for normal development of the auditory brainstem. *J. Neurosci.* 31, 8280–8294. doi: 10.1523/JNEUROSCI.5098-10.2011
- Hirtz, J. J., Braun, N., Griesemer, D., Hannes, C., Janz, K., Lohr, S., et al. (2012). Synaptic refinement of an inhibitory topographic map in the auditory brainstem requires functional Cav1.3 calcium channels. *J. Neurosci.* 32, 14602–14616. doi: 10.1523/JNEUROSCI.0765-12.2012
- Jae Huh, W., Mysorekar, I. U., and Mills, J. C. (2010). Inducible activation of Cre recombinase in adult mice causes gastric epithelial atrophy, metaplasia, and regenerative changes in the absence of “floxed” alleles. *Am. J. Physiol. Gastrointest. Liver Physiol.* 299, G368–G380. doi: 10.1152/ajpgi.00021.2010
- Janbandhu, V., Moik, D., and Fässler, R. (2014). Cre recombinase induces DNA damage and tetraploidy in the absence of LoxP sites. *Cell Cycle* 13, 462–470. doi: 10.4161/cc.27271
- Johnson, S. L., Ceriani, F., Houston, O., Polishchuk, R., Polishchuk, E., Crispino, G., et al. (2017). Connexin-mediated signaling in nonsensory cells is crucial for the development of sensory inner hair cells in the mouse cochlea. *J. Neurosci.* 37, 258–268. doi: 10.1523/JNEUROSCI.2251-16.2016
- Johnson, S. L., Eckrich, T., Kuhn, S., Zampini, V., Franz, C., Ranatunga, K. M., et al. (2011). Position-dependent patterning of spontaneous action potentials in immature cochlear inner hair cells. *Nat. Neurosci.* 14, 711–717. doi: 10.1038/nn.2803
- Johnson, S. L., Kuhn, S., Franz, C., Ingham, N., Furness, D. N., Knipper, M., et al. (2013a). Presynaptic maturation in auditory hair cells requires a critical period of sensory-independent spiking activity. *Proc. Natl. Acad. Sci. U.S.A.* 110, 8720–8725. doi: 10.1073/pnas.1219578110
- Johnson, S. L., Wedemeyer, C., Vetter, D. E., Adachi, R., Holley, M. C., Elgoyhen, A. B., et al. (2013b). Cholinergic efferent synaptic transmission regulates the maturation of auditory hair cell ribbon synapses. *Open Biol.* 3:130163. doi: 10.1098/rsob.130163
- Kiang, N. Y., Pfeiffer, R. R., Warr, W. B., and Backus, A. S. (1965). Stimulus coding in the cochlear nucleus. *Trans. Am. Otol. Soc.* 53, 35–58.
- Kros, C. J., Ruppersberg, J. P., and Rüscher, A. (1998). Expression of a potassium current in inner hair cells during development of hearing in mice. *Nature* 394, 281–284. doi: 10.1038/28401
- Lawoko-Kerali, G., Rivolta, M. N., and Holley, M. C. (2001). Expression of the transcription factors GATA3 and Pax2 during development of the mammalian inner ear. *J. Comp. Neurol.* 442, 378–391. doi: 10.1002/cne.10088
- Lieberman, M. C. (1978). Auditory-nerve response from cats raised in a low-noise chamber. *J. Acoust. Soc. Am.* 63, 442–455. doi: 10.1121/1.381736
- Lieberman, M. C. (1982). Single-neuron labeling in the cat auditory nerve. *Science* 216, 1239–1241. doi: 10.1126/science.7079757
- Liu, H.-S., Jan, M.-S., Chou, C.-K., Chen, P.-H., and Ke, N.-J. (1999). Is green fluorescent protein toxic to the living cells? *Biochem. Biophys. Res. Commun.* 260, 712–717. doi: 10.1006/bbrc.1999.0954
- Loonstra, A., Vooijs, M., Beverloo, H. B., Allak, B. A., Drunen, E., van Kanaar, R., et al. (2001). Growth inhibition and DNA damage induced by Cre recombinase in mammalian cells. *Proc. Natl. Acad. Sci.* 98, 9209–9214. doi: 10.1073/pnas.161269798
- Mammano, F., and Bortolozzi, M. (2018). Ca²⁺ signaling, apoptosis and autophagy in the developing cochlea: milestones to hearing acquisition. *Cell Calcium* 70, 117–126. doi: 10.1016/j.ceca.2017.05.006
- Marcotti, W., Johnson, S. L., and Kros, C. J. (2004). A transiently expressed SK current sustains and modulates action potential activity in immature mouse inner hair cells. *J. Physiol.* 560, 691–708. doi: 10.1113/jphysiol.2004.072868
- Marcotti, W., Johnson, S. L., Rusch, A., and Kros, C. J. (2003). Sodium and calcium currents shape action potentials in immature mouse inner hair cells. *J. Physiol.* 552, 743–761. doi: 10.1113/jphysiol.2003.043612
- Nemzou, N. R. M., Bulankina, A. V., Khimich, D., Giese, A., and Moser, T. (2006). Synaptic organization in cochlear inner hair cells deficient for the Cav1.3 (α1D) subunit of L-type Ca²⁺ channels. *Neuroscience* 141, 1849–1860. doi: 10.1016/j.neuroscience.2006.05.057
- Ohyama, T., and Groves, A. K. (2004). Generation of Pax2-Cre mice by modification of a Pax2 bacterial artificial chromosome. *Genesis* 38, 195–199. doi: 10.1002/gene.20017
- Oliver, D., Klocker, N., Schuck, J., Baukrowitz, T., Ruppersberg, J. P., and Fakler, B. (2000). Gating of Ca²⁺-activated K⁺ channels controls fast inhibitory synaptic transmission at auditory outer hair cells. *Neuron* 26, 595–601. doi: 10.1016/S0896-6273(00)81197-6
- Oliver, D., Knipper, M., Derst, C., and Fakler, B. (2003). Resting potential and submembrane calcium concentration of inner hair cells in the isolated mouse cochlea are set by KCNQ-type potassium channels. *J. Neurosci.* 23, 2141–2149. doi: 10.1523/JNEUROSCI.23-06-02141.2003
- Petitpré, C., Wu, H., Sharma, A., Tokarska, A., Fontanet, P., Wang, Y., et al. (2018). Neuronal heterogeneity and stereotyped connectivity in the auditory afferent system. *Nat. Commun.* 9:3691. doi: 10.1038/s41467-018-06033-3
- Platzer, J., Engel, J., Schrott-Fischer, A., Stephan, K., Bova, S., Chen, H., et al. (2000). Congenital deafness and sinoatrial node dysfunction in mice lacking class D L-type Ca²⁺ channels. *Cell* 102, 89–97. doi: 10.1016/S0092-8674(00)00013-1
- Pugach, E. K., Richmond, P. A., Azofeifa, J. G., Dowell, R. D., and Leinwand, L. A. (2015). Prolonged Cre expression driven by the α-myosin heavy chain promoter can be cardiotoxic. *J. Mol. Cell. Cardiol.* 86, 54–61. doi: 10.1016/j.yjmcc.2015.06.019
- Saam, J. R., and Gordon, J. I. (1999). Inducible gene knockouts in the small intestinal and colonic epithelium. *J. Biol. Chem.* 274, 38071–38082. doi: 10.1074/jbc.274.53.38071
- Sachs, L. (1999). *Angewandte Statistik. Anwendung statistischer Methoden*. Berlin: Springer.
- Satheesh, S. V., Kunert, K., Rüttiger, L., Zuccotti, A., Schönig, K., Friauf, E., et al. (2012). Retrocochlear function of the peripheral deafness gene *Cacna1d*. *Hum. Mol. Genet.* 21, 3896–3909. doi: 10.1093/hmg/dds217
- Scharinger, A., Eckrich, S., Vandael, D. H., Schönig, K., Koschak, A., Hecker, D., et al. (2015). Cell-type-specific tuning of Cav1.3 Ca²⁺-channels by a C-terminal automodulatory domain. *Front. Cell. Neurosci.* 9:309. doi: 10.3389/fncel.2015.00309
- Schindelin, J., Arganda-Carreras, I., Frise, E., Kaynig, V., Longair, M., Pietzsch, T., et al. (2012). Fiji: an open-source platform for biological-image analysis. *Nat. Methods* 9, 676–682. doi: 10.1038/nmeth.2019
- Schnütgen, F., Doerflinger, N., Calléja, C., Wendling, O., Chambon, P., and Ghyssels, N. B. (2003). A directional strategy for monitoring Cre-mediated recombination at the cellular level in the mouse. *Nat. Biotechnol.* 21, 562–565. doi: 10.1038/nbt811
- Schulz, T. J., Glaubitz, M., Kuhlow, D., Thierbach, R., Birringer, M., Steinberg, P., et al. (2007). Variable expression of cre recombinase transgenes precludes reliable prediction of tissue-specific gene disruption by tail-biopsy genotyping. *PLoS One* 2:e1013. doi: 10.1371/journal.pone.0001013
- Sendin, G., Bourien, J., Rassendren, F., Puel, J.-L., and Nouvian, R. (2014). Spatiotemporal pattern of action potential firing in developing inner hair cells of the mouse cochlea. *Proc. Natl. Acad. Sci. U.S.A.* 111, 1999–2004. doi: 10.1073/pnas.1319615111
- Shrestha, B. R., Chia, C., Wu, L., Kujawa, S. G., Liberman, M. C., and Goodrich, L. V. (2018). Sensory neuron diversity in the inner ear is shaped by activity. *Cell* 174, 1229.e17–1246.e17. doi: 10.1016/j.cell.2018.07.007
- Simmons, D. D. (2002). Development of the inner ear efferent system across vertebrate species. *J. Neurobiol.* 53, 228–250. doi: 10.1002/neu.10130
- Song, A. J., and Palmiter, R. D. (2018). Detecting and avoiding problems when using the Cre-lox system. *Trends Genet.* 34, 333–340. doi: 10.1016/j.tig.2017.12.008
- Sun, S., Babola, T., Pregernig, G., So, K. S., Nguyen, M., Su, S.-S. M., et al. (2018). Hair cell mechanotransduction regulates spontaneous activity and spiral ganglion subtype specification in the auditory system. *Cell* 174, 1247.e–1263.e. doi: 10.1016/j.cell.2018.07.008
- Tritsch, N. X., and Bergles, D. E. (2010). Developmental regulation of spontaneous activity in the Mammalian cochlea. *J. Neurosci.* 30, 1539–1550. doi: 10.1523/JNEUROSCI.3875-09.2010
- Wang, H. C., Lin, C.-C., Cheung, R., Zhang-Hooks, Y., Agarwal, A., Ellis-Davies, G., et al. (2015). Spontaneous activity of cochlear hair cells triggered by fluid secretion mechanism in adjacent support cells. *Cell* 163, 1348–1359. doi: 10.1016/j.cell.2015.10.070

- Weis, B., Schmidt, J., Lyko, F., and Linhart, H. G. (2010). Analysis of conditional gene deletion using probe based real-time PCR. *BMC Biotechnol.* 10:75. doi: 10.1186/1472-6750-10-75
- Willaredt, M. A., Ebbers, L., and Nothwang, H. G. (2014). Central auditory function of deafness genes. *Hear. Res.* 312, 9–20. doi: 10.1016/j.heares.2014.02.004
- Zuccotti, A., Kuhn, S., Johnson, S. L., Franz, C., Singer, W., Hecker, D., et al. (2012). Lack of brain-derived neurotrophic factor hampers inner hair cell synapse physiology, but protects against noise-induced hearing loss. *J. Neurosci.* 32, 8545–8553. doi: 10.1523/JNEUROSCI.1247-12.2012

Conflict of Interest Statement: The authors declare that the research was conducted in the absence of any commercial or financial relationships that could be construed as a potential conflict of interest.

Copyright © 2019 Eckrich, Hecker, Sorg, Blum, Fischer, Münkner, Wenzel, Schick and Engel. This is an open-access article distributed under the terms of the Creative Commons Attribution License (CC BY). The use, distribution or reproduction in other forums is permitted, provided the original author(s) and the copyright owner(s) are credited and that the original publication in this journal is cited, in accordance with accepted academic practice. No use, distribution or reproduction is permitted which does not comply with these terms.